Pivotal role of exogenous pyruvate in human natural killer cell metabolism

Nicolas Kern, Louis Picq, Ameline Hamond, Pierre Megy, Sarah Benezech, Annabelle Drouillard, Nina Lager-Lachaud, Edern Cahoreau, Marielle Moreau, Lucie Fallone, et al.

nature metabolism

Article

https://doi.org/10.1038/s42255-024-01188-4

Pivotal role of exogenous pyruvate in human natural killer cell metabolism

Received: 7 July 2023

Accepted: 20 November 2024

Check for updates

Nicolas Kern[1,2], Louis Picq[1], Ameline Hamond[1], Pierre Megy[1], Sarah Benezech[1], Annabelle Drouillard[1], Nina Lager-Lachaud[3], Edern Cahoreau[3], Marielle Moreau[2], Lucie Fallone[1], Anne-Laure Mathieu[1], Floriant Bellvert[3], Carine Nizard[2], Anne-Laure Bulteau[2], Thierry Walzer[1] & Antoine Marçais[1]

Resting natural killer (NK) cells display immediate effector functions after recognizing transformed or infected cells. The environmental nutrients and metabolic requirements to sustain these functions are not fully understood. Here, we show that NK cells rely on the use of extracellular pyruvate to support effector functions, signal transduction and cell viability. Glucose-derived carbons do not generate endogenous pyruvate. Consequently, NK cells import extracellular pyruvate that is reduced to lactate to regenerate glycolytic NAD^+ and is oxidized in the tricarboxylic acid (TCA) cycle to produce ATP. This supports serine production through phosphoglycerate dehydrogenase, a pathway required for optimal proliferation following cytokine stimulation but dispensable for effector functions. In addition, like mouse NK cells, human NK cells rely on a citrate–malate configuration of the TCA cycle that is not fed by glutamine. Moreover, supraphysiologic pyruvate concentrations dose-dependently increase the effector functions of NK cells. Overall, this study highlights the role of exogenous pyruvate in NK cell biology, providing knowledge that could be exploited to boost NK cell potential in therapeutic settings.

The importance of biosynthetic and bioenergetic metabolism in sustaining immune responses is increasingly recognized. A major goal in the field is to identify the environmental nutrients that condition the response of particular cell types and the metabolic configurations they allow. Glucose has traditionally been considered the primary fuel for lymphocytes, feeding glycolysis and the tricarboxylic acid (TCA) cycle through the mitochondrial oxidation of pyruvate, the end product of glycolysis. Glycolysis has a limited capacity to generate ATP compared with oxidative phosphorylation (OxPhos), a limitation compensated partly by its speed. In addition, it contributes essential metabolic intermediates for biosynthetic pathways such as the pentose phosphate pathway (PPP), the serine–glycine–one carbon (SGOC) pathway or lipid synthesis. This funnelling of intermediates out of glycolysis has been reported in both resting and activated lymphocytes[1,2]. Of note, glycolysis consumes NAD^+, a cofactor that must be quickly regenerated to support a number of metabolic reactions, including the SGOC pathway and glycolysis itself. Cytoplasmic replenishment of NAD^+ from its reduced form, NADH, relies on two processes: reduction of pyruvate to lactate by the enzyme lactate dehydrogenase (LDH) or through the electron transport chain using various mitochondrial shuttles. In activated T cells, the need to generate biosynthetic intermediates at a fast pace and to maintain an appropriate NAD/NADH ratio explains why glucose uptake and lactate excretion are massively increased even in the presence of oxygen, a phenomenon known as the Warburg effect[3,4].

[1]CIRI, Centre International de Recherche en Infectiologie, (Team Lyacts), Univ Lyon, INSERM, U1111, Université Claude Bernard Lyon 1, CNRS, UMR5308, ENS de Lyon, Lyon, France. [2]LVMH Recherche, Saint Jean de Braye, France. [3]Plateforme MetaToul FluxoMet (EAD13), Toulouse Biotechnology Institute, Bio & Chemical Engineering, Université de Toulouse, CNRS 5504, INRA 792, INSA TBI, INSA Toulouse, Toulouse, France. e-mail: thierry.walzer@inserm.fr; Antoine.marcais@inserm.fr

Consequent to lactate excretion, glucose-derived carbons are diverted away from the TCA cycle, which must then be fed by alternative nutrients. In activated T cells, the main nutrient fulfilling this anaplerotic role is glutamine through glutaminolysis; however, recent findings demonstrated that other physiologic carbon sources, including lactate and ketones, contribute to TCA cycle replenishment[2,5,6]. In addition, in various memory T cell subsets, the TCA cycle can be fed by fatty acids, although the physiological relevance of this is unclear[7,8]. Finally, SGOC metabolism has emerged early as a key metabolic node in proliferating T cells, providing necessary building blocks for de novo nucleotide synthesis[9,10]. In contrast to this wealth of data, natural killer (NK) cell metabolism has received less attention. NK cells are innate lymphocytes that display immediate effector functions even in the resting state. Indirect evidence suggests that their basal bioenergetic metabolism is rather low[11–14] and depends on mitochondrial activity in both humans and mice[15,16]. However, most studies performed to date have used cells activated by high-dose cytokine treatment for several days, whereas much less is known about resting NK cells—that is, untouched NK cells freshly isolated from the blood and not purposely stimulated. Besides, the identity of the mitochondrial fuels, the molecular links between glycolysis and OxPhos, and the relevance of the SGOC pathway in NK cells are unknown. Here, we investigated the carbon sources required by resting NK cells and how they fuel basal NK cell metabolism to sustain their immediate functions.

Results

Exogenous pyruvate conditions NK cell responses

We first tested the relative roles of three circulating primary carbon sources—glucose, glutamine and pyruvate—in sustaining NK cell functions. To keep cells as close as possible to their physiological state, we sorted resting CD56^{dim} NK cells from the blood of healthy donors (see the experimental set-up in Extended Data Fig. 1a) and cultured them without overt cytokine stimulation but with low-dose interleukin-15 (IL-15) to maintain cell viability. We then deprived cells of the different fuels one by one (glucose, pyruvate or glutamine) or treated them with BPTES, an inhibitor of glutaminolysis, before stimulation with the lymphoblastic cell line K562, a classic NK cell target. The analysis of interferon-γ (IFNγ) and macrophage inflammatory 1β (MIP1β) production and degranulation capacities (CD107a surface exposure) showed that all three functions were abrogated by the absence of pyruvate, whereas they persisted despite the shortage of glucose and glutamine or the inhibition of glutaminolysis (Fig. 1a and Extended Data Fig. 1b). In addition, the stimulation of cytokine production by IL-12/IL-18 was equally sensitive to pyruvate shortage (Extended Data Fig. 1c). We also measured NK cell cytotoxicity towards K562 cells using a technique adapted to low cell numbers[17]. Lack of pyruvate abrogated NK cell cytotoxicity, whereas glucose and glutaminolysis were dispensable (Fig. 1b). We then assessed the capacity of NK cells to respond to IL-15, as signal transduction downstream of surface receptors is conditioned by an appropriate bioenergetic metabolism[18]. As depicted in Fig. 1c, the phosphorylation of STAT5, S6 and AKT in response to IL-15 was diminished in the absence of pyruvate, whereas the absence of glucose did not significantly affect signalling. The absence of glutamine or the inhibition of glutaminolysis negatively affected only S6 phosphorylation. Moreover, the absence of exogenous pyruvate prevented the ability of IL-15 to preserve NK cell viability (Fig. 1d). In contrast, glucose deprivation did not significantly decrease survival compared with the complete medium condition. Of note, cells did not yet enter apoptosis after a 4-h culture in the absence of pyruvate (Extended Data Fig. 1d). Taken together, these results reveal a profound impact of exogenous pyruvate on human NK cell survival and effector functions.

Exogenous pyruvate controls resting NK cells' bioenergetics

Next, the impact of the different fuels on the bioenergetic metabolism of resting NK cells was measured using extracellular flux analysis (EFA). As expected, the absence of glucose resulted in a drop in baseline and maximal glycolysis as measured by the extracellular acidification rate (ECAR) (Fig. 2a–c). Of note, the ECAR is indeed an indicator of glycolytic activity as it was abrogated by treatment with 2-deoxyglucose (Fig. 2a). In contrast, the absence of glucose did not alter the baseline oxygen consumption rate (OCR) (Fig. 2d,e), suggesting that the TCA cycle was fed by alternative metabolites. Glutamine can fulfil such an anaplerotic role; however, its absence or the inhibition of glutaminolysis using BPTES did not significantly affect the OCR, suggesting that it is poorly used by resting human NK cells (Fig. 2d–g and Extended Data Fig. 2a–e). In contrast, the absence of pyruvate resulted in a significant drop in the OCR (Fig. 2d–g), suggesting that pyruvate is the preferred carbon source feeding the TCA cycle in NK cells. Unexpectedly, pyruvate shortage also negatively affected both the basal and maximal ECAR, indicating a role in sustaining glycolysis (Fig. 2a–c). Thus, pyruvate was the only fuel tested that affected both bioenergetic pathways (Fig. 2h). As a result, the absence of exogenous pyruvate specifically led to a rapid and sustained decrease in the ATP level and ATP/ADP ratio as well as a decreased production rate (Fig. 2i,j and Extended Data Fig. 2f,o). In contrast, the absence of glucose or glutamine or the inhibition of glutaminolysis did not affect the ATP level (Fig. 2i and Extended Data Fig. 2f,g). A decrease in the ATP/ADP ratio usually leads to the production of AMP by adenylate kinase, which, in turn, activates the AMP-activated protein kinase (AMPK)[19]. Surprisingly, pyruvate shortage did not result in a significant increase in AMP or AMPK activity, as measured by its phosphorylation on Thr172 or the phosphorylation of acetyl coenzyme A (acetyl-CoA) carboxylase (ACC), its canonical target (Extended Data Fig. 2i–l). Glycolysis and OxPhos act on the redox status of the NAD–NADH couple in opposite ways. Thus, we tested the impact of the three fuels on the NAD/NADH ratio and found that exogenous pyruvate was required to maintain it, in accordance with published literature[20,21], whereas no impact of glucose nor glutamine was detected (Fig. 2k). Of note, the impact of pyruvate on the ECAR and OCR parameters was reduced compared with glucose in in vitro-activated NK cells (Extended Data Fig. 2m,n), suggesting that the need for exogenous pyruvate is specific to resting NK cells. Overall, these results show that extracellular pyruvate is required to maintain bioenergetic metabolism, ATP content and NAD$^+$ levels in resting NK cells. These results explain the extreme impact of pyruvate shortage on NK cell functions.

Glucose and pyruvate fuel complementary metabolic pathways

To identify the metabolic pathways affected by exogenous pyruvate, we performed metabolomics analysis of resting NK cells cultured in the presence or absence of pyruvate. We first quantified glucose and pyruvate consumption and lactate excretion by nuclear magnetic resonance (NMR) methods. We detected pyruvate consumption, whereas glucose consumption was too limited to be significant (Fig. 3a). The absence of exogenous pyruvate did not affect glucose consumption but led to a decreased excretion of lactate (Fig. 3a,b), confirming the ECAR data. To track the source of lactate, we cultured resting NK cells with [U-^{13}C] glucose. The proportion of lactate labelled with glucose-derived ^{13}C increased from 20% in complete medium to 75% in the absence of pyruvate (Fig. 3c), showing that lactate generation from glucose-derived carbons is limited in the presence of exogenous pyruvate and suggesting that its absence partially redirects glucose-derived carbons. To investigate this point further, we quantified glucose-derived ^{13}C incorporation in carbohydrate metabolic pathways by mass spectrometry (MS). Early glycolytic intermediates were predominantly detected as fully labelled isotopologues demonstrating functional glycolysis (Fig. 3d and Extended Data Fig. 3a). In addition, intermediates of the PPP, an important source of NADPH and nucleotide precursors branching off glycolysis, were also pervasively labelled in the presence of [^{13}C] glucose (Fig. 3d and Extended Data Fig. 3a). The absence of exogenous

https://doi.org/10.1038/s42255-024-01188-4

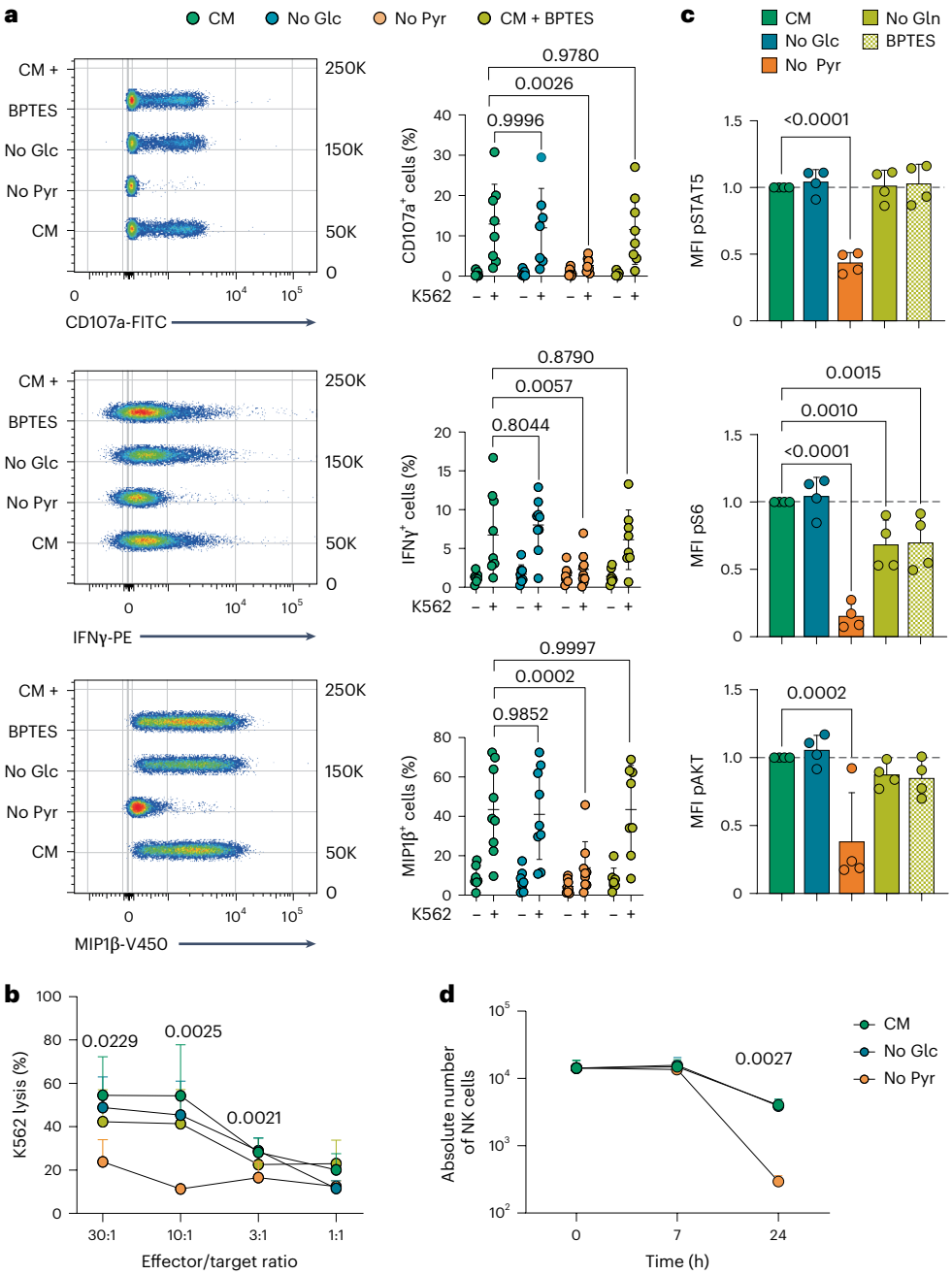

Fig. 1 | Pyruvate but not glucose depletion negatively affects NK cells. **a**,**b**, Sorted CD56^{dim} NK cells were preincubated in complete medium (CM), without glucose (no Glc), without pyruvate (no Pyr) or with BPTES (CM + BPTES) for 3 h and incubated with K562 cells expressing the NanoLuc luciferase for 4 h. The proportion of cells positive for CD107a, IFNγ and MIP1β was measured by flow cytometry. Representative dot plots (left) and the proportion of positive cells (mean ± s.d.) for each experiment (right, $n = 8$ independent donors) are shown (**a**). The percentage of K562 lysis, calculated as explained in the Methods (mean ± s.d., $n = 6$ independent donors), is shown for the indicated effector/target ratio (**b**). **c**, Sorted CD56^{dim} NK cells were cultured for 4 h in the indicated medium. No Gln, without glutamine. The mean fluorescence intensity (MFI) of pSTAT5, pS6 and pAKT S473 was measured by flow cytometry and normalized to the complete medium condition for each experiment. The mean fluorescence intensity (mean ± s.d.) in independent donors ($n = 4$) is shown. **d**, Sorted CD56^{dim} NK cells were cultured in the indicated medium for 24 h. The absolute numbers of live NK cells (mean ± s.d., $n = 3$ independent donors) measured by flow cytometry are shown. Individual points representing independent donors are shown in **a** and **c**. In **a**–**c**, one-way ANOVA tests were performed with corrections for multiple testing. A two-tailed t test was performed comparing the complete medium and without pyruvate conditions in **d**. Exact P values are shown.

pyruvate did not significantly affect the level or labelling of glycolytic intermediates upstream of pyruvate (Fig. 3e and Extended Data Fig. 3a). Importantly, late glycolytic metabolites, such as 2-/3-phosphoglycerate (2/3PG) and especially pyruvate, were less labelled by glucose-derived carbons than upstream metabolites (Fig. 3d). Moreover, the absence of exogenous pyruvate led to a sharp decline in the quantity of intracellular pyruvate itself (Fig. 3e), suggesting that intracellular pyruvate is not generated by glycolysis but instead obtained from the extracellular environment. This was confirmed by the labelling pattern of intracellular pyruvate when analysing cells cultured in a medium containing either [^{13}C]glucose or [^{13}C]pyruvate (Fig. 3f). These data and the fact that 2/3PG was present in trace amounts (<3 pmol per million cells; Fig. 3d) suggest that glycolytic intermediates were diverted to feed adjacent anabolic pathways between fructose 1,6-bisphosphate and

https://doi.org/10.1038/s42255-024-01188-4

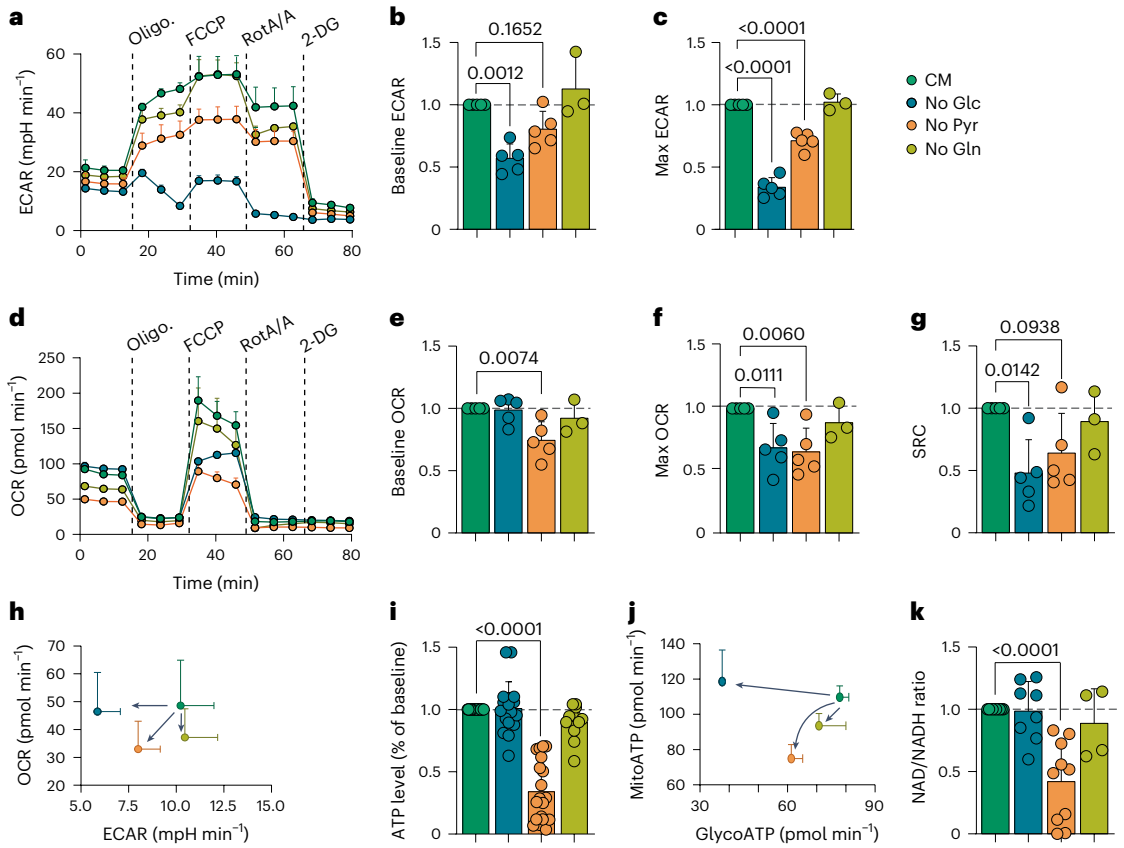

Fig. 2 | Exogenous pyruvate controls bioenergetic metabolism. a–**g**, Sorted CD56^{dim} NK cells were cultured in the indicated medium for 4 h. The ECAR (**a**–**c**) and OCR (**d**–**g**) were measured. A representative experiment (**a** and **d**) and the results (mean ± s.d.) obtained from three (no glutamine condition) to five (all other conditions) independent donors (**b**, **c**, **e**, **f** and **g**) are shown. **h**, Energetic map corresponding to the results shown in **b** and **e** (mean ± s.e.m.). **i**, ATP levels (mean ± s.d.) in 17 independent donors. **j**, ATP production rate was calculated, and a representative experiment (mean ± s.e.m., out of three independent donors) is shown. **k**, NAD/NADH ratio (mean ± s.d.) in 4 (no glutamine condition) to 10 (all other conditions) independent donors. Individual points representing independent donors are shown in **b**, **c**, **e**, **f**, **g**, **i** and **k**. One-way ANOVA tests were performed with corrections for multiple testing in **b**, **c**, **f** and **g**. Two-tailed *t* tests were performed comparing the indicated conditions in **e**, **i** and **k**. Exact *P* values are shown. Oligo., oligomycin; RotA/A, rotenone A and antimycin; 2-DG, 2-deoxyglucose; SRC, spare respiratory capacity.

pyruvate, thus limiting the endogenous production of the latter and explaining the reliance of NK cells on exogenous pyruvate. The SGOC pathway that branches off glycolysis at the 3PG stage could be responsible for this leak. This hypothesis was supported by the expression of phosphoglycerate dehydrogenase (PHGDH), the enzyme initiating the SGOC pathway (Fig. 3g). Furthermore, we observed that the quantity of phosphoserine, the product of PHGDH, as well as serine itself, the first product of SGOC, was reduced in the absence of pyruvate (Fig. 3h and Extended Data Fig. 3b). Moreover, treating the cells with PKUMDL-WQ-2101 (hereafter PKUM), a specific, allosteric inhibitor of PHGDH[22] (Extended Data Fig. 3c), restored ATP and NAD^+ levels as well as NK cell effector capacities in the absence of pyruvate (Fig. 3i and Extended Data Fig. 3d,e). Altogether, these results demonstrate the influence of this pathway on the redox and bioenergetic equilibria and, ultimately, the effector potential of resting NK cells. We next investigated the cellular fate of exogenous pyruvate. In complete medium, around half of the excreted lactate was labelled when [U-^{13}C]pyruvate was provided to NK cells (Fig. 3c), indicating that exogenous pyruvate is reduced to lactate by LDH (Fig. 3g). As pyruvate can feed the TCA cycle, we measured the labelling of TCA cycle intermediates. As shown in Fig. 3j (left), TCA cycle intermediates were only marginally labelled by glucose-derived carbons when exogenous pyruvate was present. Instead, these intermediates were labelled when [^{13}C]pyruvate was provided (Fig. 3j (right) and Extended Data Fig. 3a), confirming that exogenous pyruvate is the preferred carbon source entering mitochondria. Interestingly, labelling was limited to citrate, isocitrate and malate, a pattern reminiscent of the citrate–malate shuttle (CMS) previously described in murine NK cells[16]. Absolute quantification of the TCA cycle intermediates confirmed these findings, showing an imbalance between the different intermediates, with a far greater concentration of citrate and malate compared with α-ketoglutarate and succinate (Fig. 3k). Of note, the absence of exogenous pyruvate led to a decline in citrate concentration, which resulted in proportionally higher labelling of this metabolite by glucose-derived carbons (Fig. 3j (middle),k and Extended Data Fig. 3a). Importantly, the decrease in citrate levels observed in the absence of pyruvate was abolished by PHGDH inhibition, whereas lactate levels were not significantly affected, indicating that the carbon flux feeding the SGOC pathway can be specifically redirected towards the TCA cycle (Fig. 3k and Extended Data Fig. 3f). Pyruvate can enter the TCA cycle by carboxylation to generate oxaloacetate or decarboxylation by pyruvate dehydrogenase (PDH) to generate acetyl-CoA. The isotopologue enrichment observed for citrate and malate (m + 2) (Extended Data Fig. 3a) suggested that pyruvate entered the TCA cycle through the generation of acetyl-CoA. This was confirmed by the fact that PDH inhibition using devimistat completely abolished mitochondrial respiration as measured by a Seahorse assay (Extended Data Fig. 3g). Overall, these data show that pyruvate production through glycolysis is limited. As a result, endogenous pyruvate is not sufficient to sustain the TCA cycle and lactate production in resting NK cells, thus explaining their need for an exogenous source of this

https://doi.org/10.1038/s42255-024-01188-4

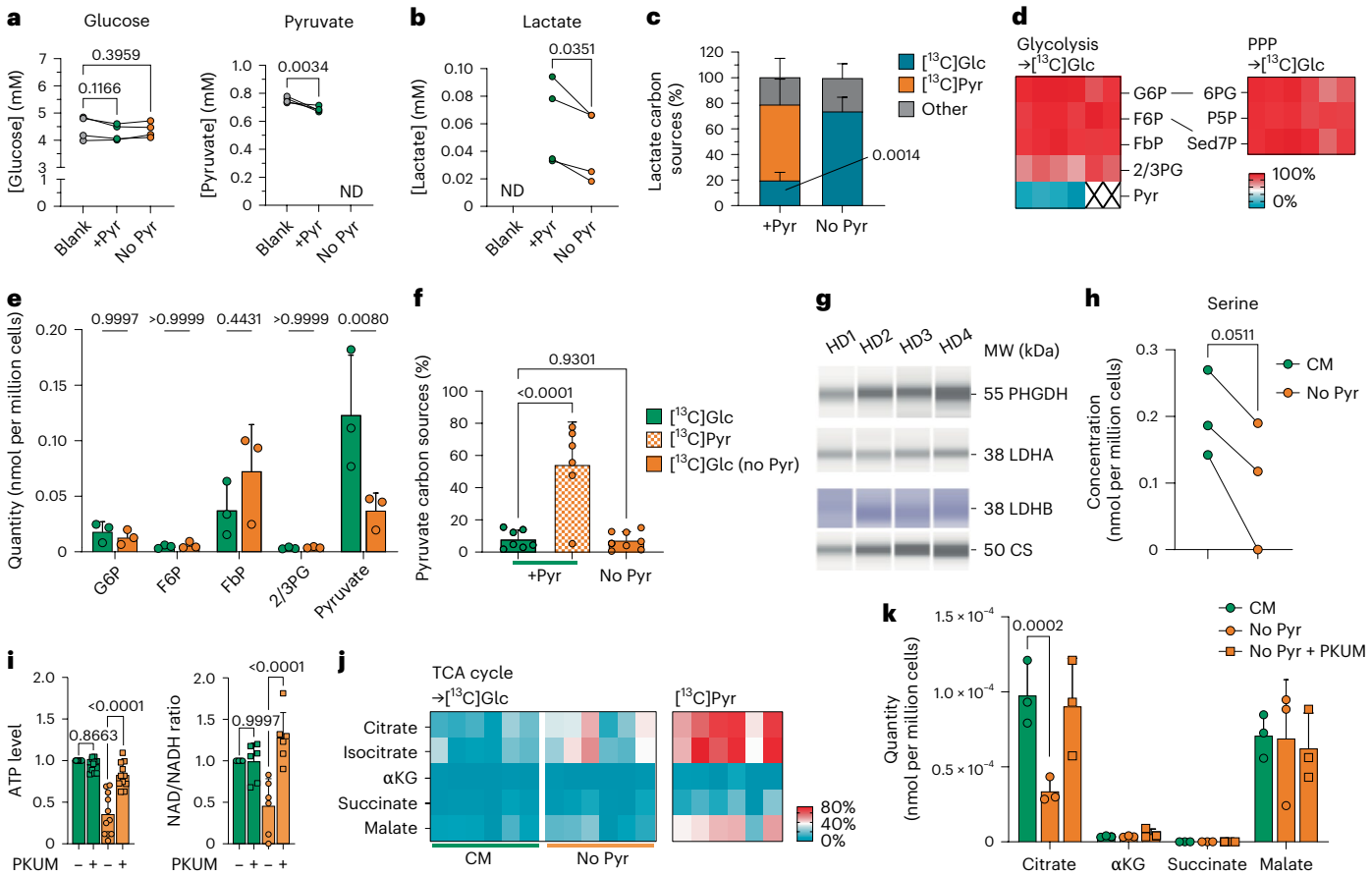

Fig. 3 | Pyruvate has a pivotal role in maintaining metabolic homoeostasis in NK cells. a,**b**, Sorted CD56^{dim} NK cells were cultured for 4 h in the indicated medium, and glucose and pyruvate (**a**) or lactate (**b**) were quantified from supernatants by NMR. Wells cultured without cells were used as blanks. Values from four independent donors are shown. Sorted CD56^{dim} NK cells were cultured for 4 h in the presence of [^{13}C]glucose or [^{13}C]pyruvate. **c**, Lactate labelling (mean ± s.d., $n = 4$ independent donors) measured by NMR. **d**, Heatmap depicting the relative contribution of [^{13}C]glucose to the indicated metabolites of glycolysis and the PPP ($n = 6$ independent donors), measured by MS. **e**, Total abundance of the indicated metabolites in NK cells cultured with or without pyruvate, measured by MS. Absolute quantities (mean ± s.d., $n = 3$ independent donors) are shown. **f**, Pyruvate labelling (mean ± s.d., $n = 7$, 6 and 8 independent donors for the [^{13}C]glucose in the presence of exogenous pyruvate, [^{13}C]pyruvate, and [^{13}C]glucose in the absence of exogenous pyruvate conditions, respectively) measured by MS. **g**, Expression of the indicated proteins on freshly sorted CD56^{dim} NK cells, measured by capillary western blotting ($n = 4$ independent donors). **h**, Absolute serine abundance in sorted CD56^{dim} NK cells cultured with or without pyruvate, measured by MS ($n = 3$ independent donors). **i**, ATP level and NAD/NADH ratio (mean ± s.d., $n = 11$ independent donors for ATP and $n = 6$ independent donors for the NAD/NADH ratio) measured in sorted CD56^{dim} NK cells cultured in the indicated medium for 4 h. **j**, Heatmap depicting the relative contribution of [^{13}C]glucose (with pyruvate (left) or without pyruvate (middle)) or [^{13}C]pyruvate (right) to the indicated metabolites of the TCA cycle ($n = 6$ independent donors). **k**, Total abundance of the indicated TCA metabolites in NK cells cultured with or without pyruvate and with or without PKUM, measured by MS. Absolute quantities (mean ± s.d., $n = 3$ independent donors) are shown. Individual points representing independent donors are shown in **a**, **b**, **e**, **f**, **h**, **i** and **k**. One-way ANOVA tests were performed with corrections for multiple testing in **a**, **e**, **f** and **i**. Two-tailed t tests were performed comparing the indicated conditions in **a**, **b**, **c**, **h** and **k**. Exact P values are shown. ND, not detected; MW, molecular mass; CS, citrate synthase; 6GP, glucose 6-phosphate; F6P, fructose 6-phosphate; FbP, fructose 1,6-bisphosphate; 6PG, 6-phosphogluconate; P5P, pentose 5-phosphate; Sed7P, sedoheptulose 7-phosphate; αKG, α-ketoglutarate.

metabolite. Our data suggest that the limited pyruvate production is due to a diversion of carbon fluxes towards serine synthesis.

Pyruvate oxidation maintains ATP and effector functions

To test how pyruvate maintains NAD$^+$ and ATP levels, we treated NK cells with GSK-2837808A (hereafter GSK, an inhibitor of LDHA and glycolysis) or oligomycin (an inhibitor of mitochondrial ATP synthase and OxPhos). As depicted in Fig. 4a, LDH inhibition reduced the NAD/NADH ratio to the levels measured following pyruvate deprivation, whereas the effect of oligomycin was milder. Partial inhibition of mitochondrial metabolism by inhibiting PDH using devimistat or the CMS using BMS-303141 similarly had no effect on the NAD/NADH ratio (Extended Data Fig. 4a). These data suggest that the NAD$^+$ pool was maintained primarily by the reduction of pyruvate to lactate in the cytoplasm. Supporting this hypothesis, α-ketobutyrate, a keto acid that can act as a substrate for LDH[23], fully complemented the absence of pyruvate and allowed NAD$^+$ regeneration (Fig. 4b). Regarding ATP levels, GSK and oligomycin separately had a moderate effect when the cells were grown in complete medium (Fig. 4c). Similarly, PDH or CMS inhibition did not affect ATP levels (Extended Data Fig. 4b). In contrast, in the absence of glucose, oligomycin treatment led to a near disappearance of ATP similar to what was observed in the absence of pyruvate. Of note, NK cell functions were spared by LDH or CMS inhibition but inhibited by oligomycin or devimistat treatment (Fig. 4d,e and Extended Data Fig. 4c). Taken together, these results suggest that pyruvate primarily sustains NAD$^+$ replenishment through LDH and ATP generation by OxPhos. However, in the absence of stimulation, glycolysis can compensate for OxPhos inhibition to maintain ATP levels when glucose is present, further underlining the plasticity of glucose usage by NK cells.

https://doi.org/10.1038/s42255-024-01188-4

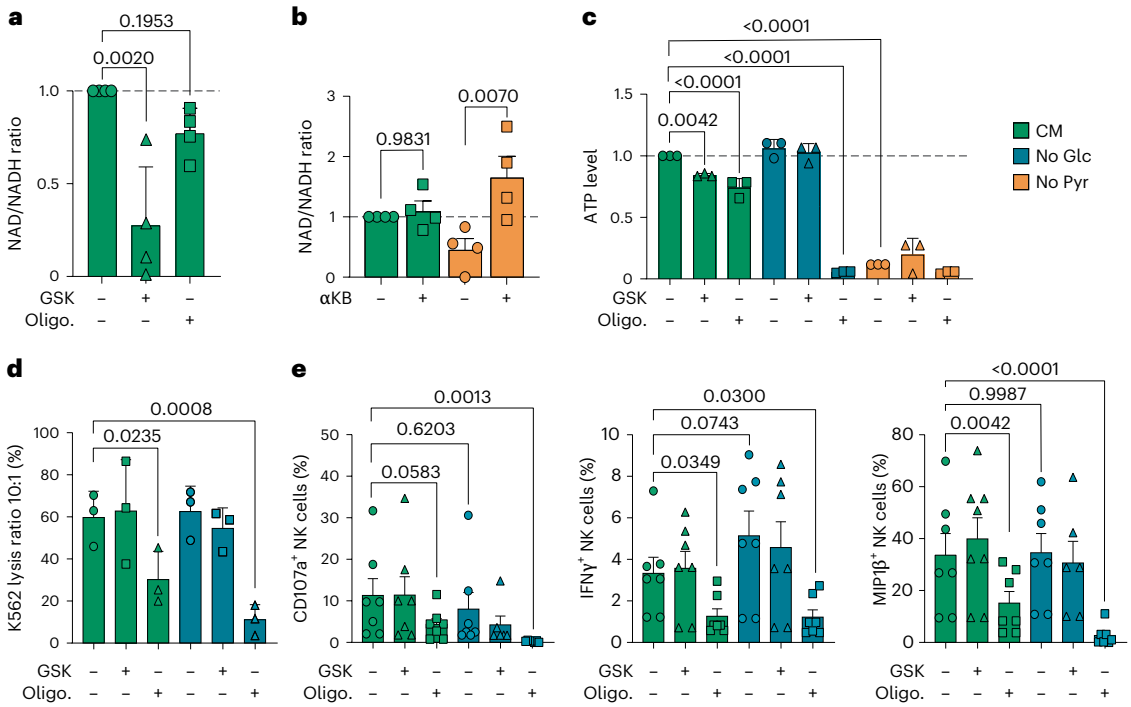

Fig. 4 | Pyruvate oxidation in the TCA cycle maintains ATP levels and effector functions. a–**c**, Sorted CD56^{dim} NK cells were cultured for 4 h in the indicated medium. The NAD/NADH ratio (mean ± s.d., $n = 4$ independent donors) is shown (**a**, **b**). αKB, α-ketobutyrate. The ATP levels (mean ± s.d., $n = 3$ independent donors) are shown (**c**). **d**,**e**, Sorted CD56^{dim} NK cells were preincubated in the indicated medium for 3 h and incubated with K562 cells expressing the NanoLuc luciferase for 4 h. The percentage of K562 lysis (mean ± s.d., $n = 3$ independent donors) is shown for the 10:1 effector/target ratio (**d**). The proportion of cells expressing CD107a, IFNγ and MIP1β measured by flow cytometry (mean ± s.e.m., $n = 7$ independent donors) is shown (**e**). Individual points representing independent donors are shown. One-way ANOVA tests were performed with corrections for multiple testing in all panels. Exact *P* values are shown.

Physiological relevance of the findings

Pyruvate is present in the blood at relatively low concentrations (40–150 µM). We wondered whether this concentration is sufficient to sustain NK cell metabolism and function. To address this question, we cultured sorted NK cells in a medium containing a dose range of pyruvate spanning physiological values. As shown in Fig. 5a–d, physiological pyruvate concentrations consistently improved the readout tested compared with the absence of pyruvate. However, supraphysiological pyruvate concentrations boosted NK cell capacities. Thus, physiological pyruvate concentrations are in the dynamic range of the sensitivity of NK cells, allowing them to sense variations in this metabolite. β-Hydroxybutyrate (another keto acid) and lactate, both present in the circulation, were observed to feed the TCA cycle in effector CD8$^+$ T cells through acetyl-CoA generation[5,6]. However, they were unable to complement the absence of pyruvate in NK cells (Extended Data Fig. 5a–d). We next decided to test the role of the SGOC pathway for NK cell functions in a medium with or without serine. As shown earlier, 4-h PHGDH inhibition did not affect the immediate functions of NK cells (Fig. 5e and Extended Data Fig. 3d,e); this result was not influenced by the presence of serine in the extracellular medium or by overnight inhibition of PHGDH before stimulation (Fig. 5e). Following cytokine stimulation, NK cells become activated and proliferate, a characteristic harnessed in the context of immunotherapies. Indeed, following stimulation with a cocktail of IL-15 and IL-18, purified NK cells proliferated vigorously, as demonstrated by the dilution of the cell trace violet dye (Fig. 5f,g). The presence of PKUM or the absence of serine in the medium inhibited this response, displaying an additive effect. Importantly, PHGDH inhibition and serine deprivation were not toxic as they prevented NK cell proliferation without affecting the survival of the undivided cells (Fig. 5h). Altogether, these results underline the nonredundant roles of de novo serine synthesis and uptake from the extracellular medium for optimal NK cell proliferation.

Discussion

Resting NK cells display immediate effector functions without the need for prior priming. Thus, in contrast to T and B cells that engage in metabolic reprogramming before acquiring their functions, NK cell functions must be sustained by the cells' basal metabolism. Despite this, NK cell metabolism has received little attention, perhaps owing to the difficulty of isolating these cells in sufficient numbers for metabolic studies. In this study, we addressed the fuel requirements of resting NK cells. We showed that resting human NK cells are functionally auxotrophic for pyruvate, the end product of glycolysis. Indeed, the absence of exogenous pyruvate results in a concomitant decrease in glycolysis and OxPhos, causing a rapid drop in ATP levels. As a consequence, an exogenous supply of pyruvate is required to sustain immediate NK cell effector functions against a tumoral cell line. In addition, survival and signal transduction are also negatively affected by the absence of pyruvate. Interestingly, variations in cytoplasmic ATP concentrations have been previously associated with signalling defects of the PI3K/AKT pathway, with PIK3δ—the PI3K isoform expressed in lymphocytes—presenting an elevated K_m for ATP (118 µM)[18]. The 60–70% decrease we report here would bring the global cellular ATP concentration around that value, which may explain the decrease in S6 and AKT phosphorylation. Whether local variations in ATP concentration could be more drastic and reach the K_m of JAK1 (15 µM)[24], the kinase responsible for signal transducer and activator of transcription 5 (STAT5) phosphorylation in NK cells, would require further investigation. Importantly, the drop in ATP levels we observed did not lead to an increase in AMP levels or activation of AMPK, suggesting that it was not properly sensed, ultimately leading to cell death. Whether this is due to suboptimal activity of sensors such as adenylate kinase (responsible for AMP generation) or other mechanisms such as direct inhibition of AMPK by increased concentrations of fructose 1,6-bisphosphate[25] is currently unknown.

https://doi.org/10.1038/s42255-024-01188-4

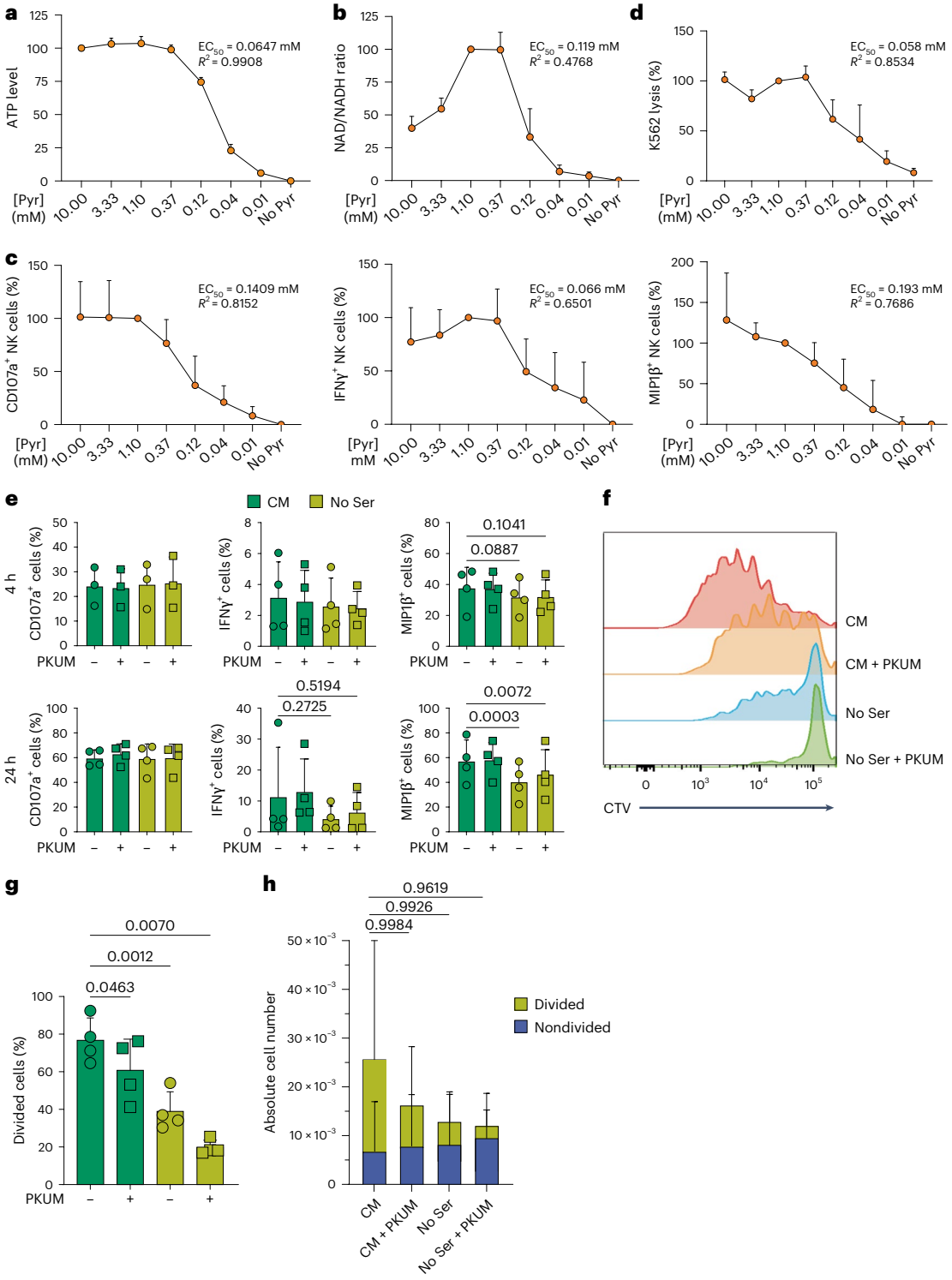

Fig. 5 | Impact of exogenous pyruvate dosage and role of SGOC. a,**b**, Sorted CD56^{dim} NK cells were cultured for 4 h in the indicated medium. The normalized ATP level (mean ± s.e.m., $n = 3$ independent donors) is shown (**a**). The normalized NAD/NADH ratio (mean ± s.e.m., $n = 3$ independent donors) is shown (**b**). **c**,**d**, Sorted CD56^{dim} NK cells were cultured for 3 h in the indicated medium. The cells were then stimulated for 4 h with K562 cells. The proportion of cells expressing CD107a, IFNγ and MIP1β measured by flow cytometry (mean ± s.e.m., $n = 4$ independent donors) is shown (**c**). The percentage of K562 lysis (mean ± s.e.m., $n = 3$ independent donors) is shown for the 10:1 effector/target ratio (**d**). The calculated EC_{50} and R^2 values are indicated (**a**–**d**). **e**, NK cells were cultured for 4 or 24 h in a medium with or without serine and in the presence or absence of PKUM. The proportion of cells positive for CD107a, IFNγ and MIP1β measured by flow cytometry (mean ± s.d., $n = 4$ independent donors, except for CD107a at 4 h ($n = 3$ independent donors)) after 4 h of K562 stimulation is shown. **f**–**h**, Resting NK cells labelled with cell trace violet (CTV) were stimulated with IL-15/IL-18 in a medium with or without serine and in the presence or absence of PKUM and analysed by flow cytometry after 5 days. A representative FACS histogram overlay out of four independent experiments is shown (**f**). The proportion of divided cells (mean ± s.e.m., $n = 4$ independent donors) measured by flow cytometry in the indicated condition is shown (**g**). The number of undivided and divided cells (mean ± s.d., $n = 4$ independent donors) counted by flow cytometry in the indicated condition is shown (**h**). One-way ANOVA tests were performed with corrections for multiple testing in **e**, **g** and **h**. Exact *P* values are shown.

Our results also suggest that glucose is not needed, at least temporarily, to sustain the effector functions of NK cells. A similar conclusion was reached in a previous study in humans, whereas the opposite was shown in murine NK cells[14,26]. The reason for this discrepancy is unclear but could stem from a disparity in the respective organ of origin of the cells or specific experimental conditions. Interestingly, stimulation results in a rapid metabolic shift characterized by high dependence on glucose[13]. The mechanisms explaining the initial steps of this reprogramming are mostly unknown. In naive T cells, a large pool of preexisting glycolytic enzymes and the mRNA for hexokinase 2 ensure a rapid onset of glycolysis[27]. Other regulatory steps, such as post-translational activation of glycolytic enzymes, have also been described[28,29]. The mechanisms at play in NK cells remain to be deciphered.

The apparent paradox of the end product of glycolysis being required exogenously to sustain the ECAR is explained by the fact that NK cells do not generate pyruvate. Indeed, metabolomics data show that less than 10% of endogenous pyruvate originates from glucose. Instead, they indicate that glycolytic intermediates are funnelled out of glycolysis, thus preventing the production of endogenous pyruvate (Extended Data Fig. 5e). Interestingly, several lines of evidence point to the SGOC pathway as a major leak point upstream of pyruvate generation. Indeed, fructose 1,6-bisphosphate is abundant, whereas 2/3PG is not, which would be consistent with an exit of glucose-derived carbons between these two points, where SGOC originates. Citrate levels are restored by SGOC inhibition, supporting the hypothesis that glucose-derived carbons are directed to the SGOC pathway instead of feeding the TCA cycle unless SGOC is inhibited. The fact that we did not detect glucose-derived labelling of SGOC intermediates points towards a limited activity of this pathway in resting NK cells, an observation correlating with the low level of glucose consumption. Of note, the activity of PHGDH, the first rate-limiting enzyme of this pathway, can have a far-reaching impact on cellular metabolism even in situations of limited net output[30].

PHGDH intervenes in glycolysis downstream of GAPDH and thus after NAD^+ consumption. Moreover, it requires NAD^+ as a cofactor[31], which probably explains the decrease in serine levels when pyruvate is absent and worsens the NAD^+/NADH imbalance. Supporting this hypothesis, PKUM treatment rescued NAD^+ levels following pyruvate deprivation. In addition, inhibition of PHGDH rescued ATP levels as well as the defect in effector capacities observed in the absence of pyruvate; these effects probably rely on the observed rescue of citrate levels, allowing OxPhos to resume. Thus, it appears that SGOC is temporally dispensable for NK cell physiology.

Why is this pathway favoured in NK cells? SGOC metabolism is essential for sustaining proliferation but dispensable for the acquisition of effector functions in $CD8^+$ T cells[10]—findings that are reminiscent of our study. A limited but continuous activity of this pathway would keep NK cells poised for proliferation following stimulation, whereas overt stimulation would lead to activation. Moreover, recent data obtained in macaques suggested that peripheral NK cells are subject to more dynamic turnover in vivo than was previously appreciated[32]. In this context, continuous feeding of the SGOC pathway would sustain this homoeostatic proliferation. Another possibility would be that serine is required for the long term to sustain NK cell cytotoxicity, as suggested in a recent study underlining the role of this amino acid for the synthesis of sphingomyelin and an optimal membrane topology[33]. In addition to generating serine and glycine, SGOC metabolism is also central to cellular redox equilibrium, nucleotide synthesis and methylation reactions[31,34]. In addition, PHGDH activity could also coordinate independent pathways active in resting NK cells, such as the PPP or TCA cycle, through yet undefined mechanisms as shown in diverse tumour cell lines[30]. Identifying the underlying reason for SGOC usage in resting NK cells will require further investigation.

Consequent to the inability of NK cells to generate endogenous pyruvate, glycolysis is uncoupled from mitochondria at the cellular level in these cells, a finding well in line with recent reports[35]. However, in most studies to date, lactate and ketones have been designated as the main circulating carbon sources imported to feed the TCA cycle to generate energy[5,35,36]. Interestingly, neither lactate nor ketones can replace pyruvate in resting NK cells in our settings. Regarding lactate, we attribute this specificity to the fact that NK cells have highly restricted amounts of NAD^+ and are thus unable to reduce lactate to pyruvate before oxidation in mitochondria. Interestingly, this absolute requirement for NAD^+ replenishment is reminiscent of highly proliferating cells[4]. However, in contrast to highly metabolic cells that can increase pyruvate production to compensate for insufficient NAD^+ regeneration by mitochondria, resting NK cells are unable to do so. Therefore, they rely on surrounding cells for pyruvate supply and hence for the control of their redox status.

Exogenous pyruvate sustains both glycolysis and OxPhos. However, we observed that OxPhos has a nonredundant role in sustaining effector functions even in the presence of glucose. This agrees with earlier reports showing that mitochondrial activity is required for the functions of human NK cells[15]. EFA measurement of the ATP production rate by Seahorse assays and our data using glycolysis and OxPhos or TCA cycle inhibitors suggest that both contribute to ATP production. Thus, the role of mitochondrial ATP has to be discarded unless glycolysis and mitochondria feed distinct cellular ATP pools with separate usage, as recently proposed in T cells[18], or unless the glycolytic ATP production rate becomes limiting following stimulation. We would instead propose that mitochondrial activity could provide specific molecules (for example, ROS) required for optimal cellular response to challenge[37].

Mechanistically, the fact that the dominant citrate isotopologue is labelled as m + 2, combined with the fact that the inhibition of PDH inhibits OxPhos, indicates that pyruvate enters the TCA cycle through decarboxylation to acetyl-CoA. Moreover, the preferential labelling of citrate/isocitrate and malate by pyruvate and their net excess over α-ketoglutarate or succinate indicate that the TCA cycle is in a CMS configuration. This confirms previous reports in cytokine-activated murine NK cells[16,38] and explains why glutamine is not used as an anaplerotic substrate. Of note, we observed a limited impact of CMS inhibition on NAD^+ regeneration, underlining the nonredundant role of LDH and the importance of the cytosolic NAD^+/NADH pool. Similarly, immediate effector functions were resistant to CMS inhibition, whereas PDH or ATP synthase inhibition resulted in their repression. We interpret these results as denoting the plasticity of the TCA cycle configuration in human NK cells.

Interestingly, our data showed that the EC_{50} of pyruvate in vitro was above or around the physiologic range of pyruvate serum concentrations for the different readouts. This suggests that NK cells operate well below their maximal capacities at physiological pyruvate concentrations and can unfold spare effector capacities in the presence of supraphysiologic concentrations of pyruvate. In the context of cellular therapy, this could orient future therapeutic developments.

Methods

The research reported in this article complies with all relevant French ethical regulations (under the convention EFS 16-2066).

Human samples

Peripheral blood samples from healthy participants were obtained from the French blood agency (Etablissement Français du sang, Lyon, France) after the donors' informed consent had been obtained. Human peripheral blood mononuclear cells (PBMCs) were separated from peripheral blood by Ficoll gradient centrifugation (Eurobio Laboratoires et AbCys) at room temperature. PBMCs were kept overnight in complete medium at 4 °C.

NK cell sorting and culture

For the isolation of $CD56^{dim}$ NK cells, a first step of enrichment was performed using an NK cell isolation kit (Miltenyi Biotec) following the

manufacturer's instructions. $CD56^{dim}CD3^{-}$ NK cells were then sorted (BD FACS Aria II, purity >99%). Freshly sorted NK cells were left to recover from the sort overnight at 37 °C with a nonstimulating dose of IL-15 (1 ng ml^{-1}, Peprotech) in RPMI 1640 medium containing 10% FBS, 2 mM HEPES, 2 mM glutamine, 1 mM pyruvate and 1% penicillin/streptomycin (HCL Technologies). The following day, cells were washed twice in PBS + 0.5% BSA and resuspended in RPMI 1640 medium powder (US Biological) reconstituted following the manufacturer's instructions. The medium was supplemented with 1× amino acid solution (R7131, Sigma), 2 mM HEPES (Gibco) and 1% penicillin/ streptomycin (HCL Technologies). To avoid the addition of undefined metabolites from FBS, we complemented the medium with 0.5% BSA. Glucose (5.5 mM), pyruvate (1 mM) and glutamine (2 mM) were added or not as indicated. Low-dose IL-15 (1 ng ml^{-1}) was present in all media. Where indicated, cells were cultured with or without BPTES (10 µM), PKUM (12.5 µM), GSK (10 µM), oligomycin (1.5 µM), devimistat (150 µM), BMS-303141 (5 µM), β-hydroxybutyrate (1 mM) or α-ketobutyrate (1 mM). For survival experiments, 10,000 NK cells were plated in a 96-well culture plate in the indicated medium at 37 °C and 5% CO_2. The absolute numbers of live NK cells were counted at the indicated times by propidium iodide staining using a BD Accuri C6 Plus flow cytometer.

Long-term activation of NK cells in vitro

NK cells from whole human blood were purified using an NK cell isolation kit (Miltenyi Biotec). Purified NK cells were seeded at 10^6 cells per ml and cultured with 1,000 IU ml^{-1} IL-2 (Peprotech) in MACS medium (Miltenyi Biotec). An NK cell activation/expansion kit (Miltenyi Biotec) was used following the manufacturer's instructions at the beginning of the culture. The cells were used after at least 15 days of culture for EFA and capillary western blot analysis. For proliferation experiments, purified NK cells (NK cell isolation kit, Miltenyi Biotec) were stained with cell trace violet (Invitrogen, C34557). Cells (0.2×10^6) were seeded in the indicated medium. After 5 days, proliferation was measured by flow cytometry (MACSQuant, Miltenyi Biotec).

Flow cytometry

Cell surface staining was performed for 30 min at 4 °C in FACS buffer (PBS, 2% FBS, 2 mM EDTA). Intracellular staining of cytokines and chemokines was performed with Cytofix/Cytoperm (BD Biosciences). Intracellular staining of phosphorylated proteins was performed using Lyse/Fix and Perm III buffers (BD Biosciences). Phosphorylated proteins were then stained for 40 min at room temperature. The following monoclonal antibodies from eBioscience, BD Biosciences, BioLegend or Cell Signaling Technology were used: anti-CD56 APC (NCAM16.2, 1/50), anti-CD3 PerCPCy5.5 (UCHT1, 1/50), anti-pSTAT5 (47/Stat5(pY694), 1/40), anti-pS6 (D57.2.2E, 1/400), anti-pAKT (M89-61, 1/100), anti-IFNγ PE (4S.B3, 1/10), anti-CD107a FITC (H4A3, 1/50) and anti-MIP1β BV421 (D21-1351, 1/20). Viability staining was performed using the Live/Dead Fixable Near IR (780) viability kit (Invitrogen, 1/1,000). Sample acquisition was performed on a five-laser LSR Fortessa flow cytometer (Becton Dickinson). Data were analysed with FlowJo 10.5.0 software (Tree Star).

EFA assay

Sorted $CD56^{dim}$ NK cells were plated at 500,000 cells per well in CellTack-coated XF96 cell culture microplates and cultured for 4 h with IL-15 (1 ng ml^{-1}) in complete Seahorse XF RPMI medium (Agilent Technologies, 103576) with or without 5.5 mM glucose, 1 mM pyruvate and 2 mM glutamine. The OCR and ECAR were assessed on an XF96 Extracellular Flux Analyzer (Agilent Technologies). The OCR and ECAR were measured under basal conditions and after the sequential addition of 1.5 µM oligomycin, 3 µM carbonyl cyanide *p*-trifluoromethoxyphenylhydrazone (FCCP), 1.5 µM antimycin A + 1.5 µM rotenone and 50 mM 2-deoxyglucose (all from Sigma-Aldrich). Data were normalized to cell numbers. OxPhos, glycolysis and glycolytic capacity were calculated as follows: baseline ECAR = (last measurement before oligomycin injection − minimum rate measurement after 2-deoxyglucose injection); maximal ECAR = maximal rate measurement; basal OCR = (late rate measurement before oligomycin injection − minimum rate measurement after rotenone A and antimycin injection); maximal OCR = (maximum rate measurement after FCCP injection − minimum rate measurement after rotenone A and antimycin injection); spare respiratory capacity = (maximal OCR − basal OCR). For the ATP rate assay, mitochondrial and glycolytic ATP rates were measured using an ATP rate assay test kit (Agilent Technologies) following the manufacturer's instructions.

ATP, ATP/ADP and NAD/NADH quantification

Sorted $CD56^{dim}$ NK cells were seeded at 30,000 cells per well in 96-well plates in the indicated culture medium for 4 h. Measurements of the ATP level, ATP/ADP ratio and NAD/NADH ratio were performed using luciferase-based assays following the manufacturer's instructions (CellTiter-Glo 2.0 cell viability assay and NAD/NADH-Glo assay (Promega) and ADP/ATP ratio assay kit (Merck)). Luminescence was measured using a TriStar luminometer (Berthold Technologies).

NK cell stimulation

Sorted NK cells (1×10^5) were cultured in the indicated medium for 3 h in the presence of 1 ng ml^{-1} IL-15 and then cocultured for 4 h with K562 cells or with IL-12 (10 ng ml^{-1}) and IL-18 (50 ng ml^{-1}) in the presence of GolgiStop (BD Biosciences) for the last 3 h. The percentage of NK cells positive for CD107a, MIP1β and IFNγ was then determined by flow cytometry.

Measurement of NK cell cytotoxicity

Human PBMCs or sorted NK cells were cultured in the indicated medium for 3 h and then cocultured for 4 h at different effector/target ratios with K562 $NanoLuc^{+}$ target cells[17]. The supernatant was collected, and bioluminescence was measured using a TriStar luminometer (Berthold Technologies) after the addition of furimazine, the substrate of NanoLuc. Furimazine was generated from a hikarazine, as previously described[39,40]. The percentage of cell lysis was calculated as explained by Hayek et al.[17]. Q26

Metabolomics analysis

Sorted $CD56^{dim}$ NK cells were incubated for 4 h in a medium with or without [U-^{13}C]glucose or [U-^{13}C]pyruvate (Eurisotop). Cells were isolated by centrifugation at 14,000*g* for 5 min at 4 °C. The supernatant was collected and snap-frozen in liquid nitrogen. Cell pellets were washed two times in 1× PBS before being snap-frozen in liquid nitrogen.

Quantification and isotopic profiling of intracellular metabolites by MS. Extraction was performed as follows. Cell pellets were taken up in 1 ml acetonitrile/methanol/water + 125 mM formic acid at −20 °C (and 50 µl of isotope dilution method standard solution for absolute quantification experiments). Then, the cell suspension was vortexed, sonicated and incubated for 45 min at −20 °C. Finally, the samples were dried with SpeedVac. The samples were then recovered with 100 µl MilliQ water (amino acid and central metabolite analyses) or 25 mM ammonium formate (pH 3.0)/methanol (98:2, v/v) (CoA run or initial conditions of the hydrophilic interaction liquid chromatography (LC) run), vortexed, sonicated, centrifuged (5 min, 14,000*g*) and then transferred to a vial for MS analysis. For central metabolite quantification, extracts were analysed by ionic chromatography coupled with MS (Orbitrap Q Exactive Plus mass spectrometer, Thermo Fisher Scientific). Central metabolites were separated on an ionic chromatography column (IonPac AS11, 250 × 2 mm internal diameter; Dionex). The mobile phase used was a gradient of potassium hydroxide at a flow rate of 380 µl min^{-1}. The mobile phase was varied as follows: 0 min, 7 mM; 1 min, 7 mM; 9.5 min, 15 mM; 20 min, 15 mM; 30 min, 45 mM; 33 min, 70 mM; 33.1 min, 100 mM; and 42 min, 100 mM. The column was then Q27

equilibrated for 5 min at the initial conditions before the next sample was analysed. The duration of the analysis was 50 min. The volume of injection was 15 µl. High-resolution experiments were performed with an ICS-5000 Plus ion chromatography system (Dionex) coupled to an Orbitrap Q Exactive Plus mass spectrometer (Thermo Fisher Scientific) equipped with a heated electrospray ionization probe. MS analyses were performed in negative Fourier transform MS mode at a resolution of 70,000 (at 400 *m/z*) in full-scan mode, with the following source parameters: capillary temperature, 350 °C; source heater temperature, 350 °C; sheath gas flow rate, 50 AU (arbitrary units); auxiliary gas flow rate, 10 AU; S-lens RF level, 65%; and source voltage, 2.75 kV. Metabolites were determined by extracting the exact mass with a tolerance of 5 ppm.

For amino acid analyses, high-resolution experiments were performed with a Vanquish HPLC system connected to an LTQ Orbitrap Velos mass spectrometer (Thermo Fisher Scientific) equipped with a heated electrospray ionization probe. MS analyses were performed in positive Fourier transform MS mode at a resolution of 60,000 (at 400 *m/z*) in full-scan mode, with the following source parameters: capillary temperature, 275 °C; source heater temperature, 250 °C; sheath gas flow rate, 45 AU; auxiliary gas flow rate, 20 AU; S-lens RF level, 40%; and source voltage, 5 kV. Metabolites were determined by extracting the exact mass with a tolerance of 5 ppm.

Acetyl-CoA analyses were carried out on an LC–MS platform composed of a Thermo Scientific Vanquish Focused UHPLC Plus system coupled to a Q Exactive Plus mass spectrometer (Thermo Fisher Scientific). The analysis of short polar acyl-CoA thioesters in the samples was performed on a Phenomenex Kinetex column (100 mm × 3.0 mm; 1.7 µm). The column was kept at 25 °C, and the flow rate was set to 0.35 ml min^{-1}. The solvent system consisted of 25 mM ammonium formate in water (pH 8.0) (solvent A) and methanol (solvent B). The gradient programme started with 2% solvent B for 2 min, increasing up to 25% solvent B over 21 min; at 23.1 min, solvent B was increased up to 95% and held for 5 min for column cleaning, followed by a return to the initial condition within 0.1 min and 8 min of equilibration of the column. The injected sample volume was 5 µl, and the autosampler temperature was 4 °C. Mass detection was carried out in positive electrospray ionization mode. The settings of the mass spectrometer were as follows: spray voltage, 4.5 kV; capillary and desolvation temperature, 320 and 350 °C, respectively; and maximum injection time, 50 ms. Nitrogen was used as sheath gas (pressure 55 units) and auxiliary gas (pressure 10 units). The automatic gain control was set at 1×10^6 and a resolution of 70,000 from 300 to 1,500 *m/z*. MS analysis was performed in full-scan mode. Data acquisition was performed using Thermo Scientific Xcalibur software.

Absolute quantification. For absolute quantification of metabolites, the correlation coefficient (R^2) must be ≥0.99 for each metabolite. Their concentrations have to be included in the dynamic range of the method.

Isotopic profile analysis. For isotopic profile analysis of metabolites, their concentrations have to be included in the dynamic range of the method. This range was determined during method validation with the PA–PT sample and corresponds to the total area of the cluster/number of isotopologues with a bias of less than 5%.

Quantification and isotopic profiling of extracellular metabolites by NMR. Cultivation supernatants were sampled to measure metabolite concentrations and ^{13}C positional labelling in the medium during cultivation. A volume of 500 µl of blank medium samples (without cells) and supernatants was taken after 4 h of cell cultivation.

A volume of 180 µl of these samples was mixed with 20 µl of an internal standard consisting of 10 mM TSP-d4 (deuterated trimethylsilylpropanoic acid) diluted in D_2O. Proton NMR spectra were recorded on an Avance Neo 800-MHz spectrometer equipped with a 5-mm z-gradient QCI-P (^1H, ^{13}C, ^{15}N, ^{31}P) cryoprobe (Brucker). Quantitative ^1H-1D NMR analyses were performed at 280 K, using a zgpr30 sequence with a repetition interval of 10 s and presaturation at 4.697 ppm for water signal suppression. Sixty-four scans were accumulated (64k data points with a spectral width of 20 ppm) after four dummy scans. The spectra were processed using TopSpin 4.1.3 (Bruker). Over the different conditions, 23 metabolites in the supernatants were identified and quantified. Among them, we measured positional incorporation into two metabolites: pyruvate (C3) and lactate (C3).

Automated capillary electrophoresis western analysis

Sorted $CD56^{dim}$ NK cells were lysed in whole-cell extraction buffer (5 mM Tris–HCl, pH 7.5, 0.25 mM saccharose, 0.2 mM $MgSO_4$, 20 mM EDTA, 0.4% Triton X-100, 2 mM DTT, 5 µg ml^{-1} leupeptin, 0.4 mM PMSF). Cell lysates were sonicated for five cycles of 8 s on/30 s off with a Bioruptor Pico ultrasonicator (Diagenode) at 4 °C and then spun down for supernatant collection. Protein concentration was determined by the DC protein assay (Bio-Rad Laboratories). Protein levels were determined by capillary electrophoresis immunoassay following the Wes user guide from Protein Simple, and primary antibody dilutions were determined: anti-PHGDH rabbit (NBP1-87311, Novus Biologicals Europe, 1/80), anti-LDHA rabbit (NBP1-48336, Novus Biologicals Europe, 1/200), anti-LDHB rabbit (MAB9205-SP, R&D Systems, 1/250), anti-AMPKα (D5A2, Cell Signaling Technology, 1/50), anti-pAMPK Thr172 (40H9, Cell Signaling Technology, 1/10) and anti-pACC Ser79 (3661, Cell Signaling Technology, 1/50). Positive controls for pACC detection were generated by exposing NK cells to 1 µM MK8722 (MedChemExpress) for 1 h. After plate loading, the electrophoresis and immunodetection steps took place in the capillary system (Protein Simple Wes, Protein Simple) and were fully automated with instrument default settings. Peak areas were determined using the Compass software (Protein Simple) and normalized to citrate synthase (anti-rabbit, EPR8067, Abcam).

Measurement of intracellular serine

Cells (2.5×10^6) were lysed, and intracellular serine content was measured according to the manufacturer's instructions (MAK352, Merck).

Statistics

No statistical methods were used to predetermine sample sizes, but our sample sizes are similar to those reported in previous publications. In a given experiment, samples derived from each donor were assessed for all conditions; as no comparison between donors was performed, they were not randomized. Data collection and analysis were not performed blind to the conditions of the experiments, except for the metabolomic measurements that were performed in a totally blind fashion. No data points were excluded. Excel 16.90 (Microsoft) was used for data collection, and GraphPad Prism 9.5.1 (GraphPad Software) was used for statistical analysis. Results are expressed as the mean ± s.e.m. or mean ± s.d., as indicated in the figure legends. A two-tailed Student's *t* test was used when only two groups were compared. A one-way analysis of variance (ANOVA) test was used for the comparison of more than two groups, with the Tukey or Dunnett test for multiple comparisons. Exact *P* values are shown until they fall below 0.0001. Data distribution was assumed to be normal, but this was not formally tested.

Reporting summary

Further information on research design is available in the Nature Portfolio Reporting Summary linked to this article.

Data availability

Data supporting the findings of this study are available on request from the corresponding authors (A.M. or T.W.). Source data are provided with this paper.

References

1. Ma, R. et al. A Pck1-directed glycogen metabolic program regulates formation and maintenance of memory CD8$^+$ T cells. *Nat. Cell Biol.* **20**, 21–27 (2018).
2. Wang, R. et al. The transcription factor Myc controls metabolic reprogramming upon T lymphocyte activation. *Immunity* **35**, 871–882 (2011).
3. Ma, E. H. et al.Metabolic profiling using stable isotope tracing reveals distinct patterns of glucose utilization by physiologically activated CD8$^+$ T cells. *Immunity* https://doi.org/10.1016/j.immuni.2019.09.003 (2019).
4. Luengo, A. et al. Increased demand for NAD$^+$ relative to ATP drives aerobic glycolysis. *Mol. Cell* **81**, 691–707 (2021).
5. Kaymak, I. et al. Carbon source availability drives nutrient utilization in CD8$^+$ T cells. *Cell Metab.* **34**, 1298–1311 (2022).
6. Luda, K. M. et al. Ketolysis drives CD8$^+$ T cell effector function through effects on histone acetylation. *Immunity* **56**, 2021–2035 (2023).
7. Pan, Y. et al. Survival of tissue-resident memory T cells requires exogenous lipid uptake and metabolism. *Nature* **543**, 252–256 (2017).
8. Raud, B. et al. Etomoxir actions on regulatory and memory T cells are independent of Cpt1a-mediated fatty acid oxidation. *Cell Metab.* **28**, 504–515 (2018).
9. Ron-Harel, N. et al. Mitochondrial biogenesis and proteome remodeling promote one-carbon metabolism for T cell activation. *Cell Metab.* **24**, 104–117 (2016).
10. Ma, E. H. et al. Serine is an essential metabolite for effector T cell expansion. *Cell Metab.* **25**, 345–357 (2017).
11. Marçais, A. et al. The metabolic checkpoint kinase mTOR is essential for IL-15 signaling during the development and activation of NK cells. *Nat. Immunol.* **15**, 749–757 (2014).
12. Donnelly, R. P. et al. mTORC1-dependent metabolic reprogramming is a prerequisite for NK cell effector function. *J. Immunol.* https://doi.org/10.4049/jimmunol.1401558 (2014).
13. Keating, S. E. et al. Metabolic reprogramming supports IFN-γ production by CD56^{bright} NK cells. *J. Immunol.* **196**, 2552–2560 (2016).
14. Keppel, M. P., Saucier, N., Mah, A. Y., Vogel, T. P. & Cooper, M. A. Activation-specific metabolic requirements for NK cell IFN-γ production. *J. Immunol.* **194**, 1954–1962 (2015).
15. Surace, L. et al. Polarized mitochondria as guardians of NK cell fitness. *Blood Adv.* **5**, 26–38 (2021).
16. Assmann, N. et al. Srebp-controlled glucose metabolism is essential for NK cell functional responses. *Nat. Immunol.* **18**, 1197–1206 (2017).
17. Hayek, S. et al. Identification of primary natural killer cell modulators by chemical library screening with a luciferase-based functional assay. *SLAS Discov.* **24**, 25–37 (2019).
18. Xu, K. et al. Glycolysis fuels phosphoinositide 3-kinase signaling to bolster T cell immunity. *Science* **371**, 405–410 (2021).
19. Steinberg, G. R. & Hardie, D. G. New insights into activation and function of the AMPK. *Nat. Rev. Mol. Cell Biol.* **24**, 255–272 (2023).
20. Hung, Y. P., Albeck, J. G., Tantama, M. & Yellen, G. Imaging cytosolic NADH–NAD$^+$ redox state with a genetically encoded fluorescent biosensor. *Cell Metab.* **14**, 545–554 (2011).
21. Bücher, T. et al. State of oxidation–reduction and state of binding in the cytosolic NADH-system as disclosed by equilibration with extracellular lactate/pyruvate in hemoglobin-free perfused rat liver. *Eur. J. Biochem.* **27**, 301–317 (1972).
22. Wang, Q. et al. Rational design of selective allosteric inhibitors of PHGDH and serine synthesis with anti-tumor activity. *Cell Chem. Biol.* **24**, 55–65 (2017).
23. Sullivan, L. B. et al. Supporting aspartate biosynthesis is an essential function of respiration in proliferating cells. *Cell* **162**, 552–563 (2015).
24. Knight, Z. A. & Shokat, K. M. Features of selective kinase inhibitors. *Chem. Biol.* **12**, 621–637 (2005).
25. Zhang, C.-S. et al. Fructose-1,6-bisphosphate and aldolase mediate glucose sensing by AMPK. *Nature* **548**, 112–116 (2017).
26. Picard, L. K., Littwitz-Salomon, E., Waldmann, H. & Watzl, C. Inhibition of glucose uptake blocks proliferation but not cytotoxic activity of NK cells. *Cells* **11**, 3489 (2022).
27. Wolf, T. et al.Dynamics in protein translation sustaining T cell preparedness. *Nat. Immunol.* https://doi.org/10.1038/s41590-020-0714-5 (2020).
28. Menk, A. V. et al. Early TCR signaling induces rapid aerobic glycolysis enabling distinct acute T cell effector functions. *Cell Rep.* **22**, 1509–1521 (2018).
29. Schafer, J. R. et al.Education-dependent activation of glycolysis promotes the cytolytic potency of licensed human natural killer cells. *J. Allergy Clin. Immunol.* https://doi.org/10.1016/j.jaci.2018.06.047 (2018).
30. Reid, M. A. et al. Serine synthesis through PHGDH coordinates nucleotide levels by maintaining central carbon metabolism. *Nat. Commun.* **9**, 5442 (2018).
31. Locasale, J. W. Serine, glycine and one-carbon units: cancer metabolism in full circle. *Nat. Rev. Cancer* **13**, 572–583 (2013).
32. Wu, C. et al. Clonal expansion and compartmentalized maintenance of rhesus macaque NK cell subsets. *Sci. Immunol.* **3**, eaat9781 (2018).
33. Zheng, X. et al. Tumors evade immune cytotoxicity by altering the surface topology of NK cells. *Nat. Immunol.* **24**, 802–813 (2023).
34. Fan, J. et al. Quantitative flux analysis reveals folate-dependent NADPH production. *Nature* **510**, 298–302 (2014).
35. Hui, S. et al. Glucose feeds the TCA cycle via circulating lactate. *Nature* **551**, 115–118 (2017).
36. Hui, S. et al. Quantitative fluxomics of circulating metabolites. *Cell Metab.* **32**, 676–688 (2020).
37. Sena, L. A. et al. Mitochondria are required for antigen-specific T cell activation through reactive oxygen species signaling. *Immunity* **38**, 225–236 (2013).
38. Loftus, R. M. et al. Amino acid-dependent cMyc expression is essential for NK cell metabolic and functional responses in mice. *Nat. Commun.* **9**, 2341 (2018).
39. Coutant, E. P. et al. Gram-scale synthesis of luciferins derived from coelenterazine and original insights into their bioluminescence properties. *Org. Biomol. Chem.* **17**, 3709–3713 (2019).
40. Coutant, E. P. et al. Bioluminescence profiling of nanoKAZ/NanoLuc luciferase using a chemical library of coelenterazine analogues. *Chemistry* **26**, 948–958 (2020).

Acknowledgements

We acknowledge the contribution of the SFR Biosciences (Université Claude Bernard Lyon 1, Centre National de la Recherche Scientifique (CNRS) UAR3444, Institut National de la Santé et de la Recherche Médicale (INSERM) US8, ENS de Lyon) flow cytometry facility and the AniRA-ImmOs platform. We acknowledge the contributions of the CELPHEDIA Infrastructure (http://www.celphedia.eu/), especially the centre AniRA in Lyon. We thank R. Rossignol (INSERM-Université de Bordeaux, France) for helpful discussions. We acknowledge the contribution of the Etablissement Français du Sang Auvergne-Rhône-Alpes. The T.W. laboratory receives institutional grants from the INSERM, CNRS, Université Claude Bernard Lyon 1 and ENS de Lyon. N.K. was an employee of Parfums Christian Dior (thèse CIFRE) at the time of the study. This work was supported by a grant from LVMH-Recherche.

Author contributions

A.M. and T.W. came up with the general approach. N.K., A.M. and T.W. designed the experiments with inputs from C.N. and A.-L.B., and N.K. performed them with the help of L.P., A.H., P.M., S.B., A.D., M.M., L.F. and A.-L.M. N.L.-L., E.C. and F.B. performed the metabolomics analysis. A.M. wrote the paper with inputs from T.W. and N.K. All authors critically read the manuscript.

Competing interests

N.K. was an employee of Parfums Christian Dior at the time of the study. M.M., C.N. and A.L.B. are employees of LVMH-Recherche. The other authors declare no competing interests.

Additional information

Extended data is available for this paper at https://doi.org/10.1038/s42255-024-01188-4.

Supplementary information The online version contains supplementary material available at https://doi.org/10.1038/s42255-024-01188-4.

Correspondence and requests for materials should be addressed to Thierry Walzer or Antoine Marçais.

Peer review information *Nature Metabolism* thanks David Finlay, Lydia Lynch and Felix Wensveen for their contribution to the peer review of this work. Primary Handling Editor: Alfredo Giménez-Cassina, in collaboration with the *Nature Metabolism* team.

https://doi.org/10.1038/s42255-024-01188-4

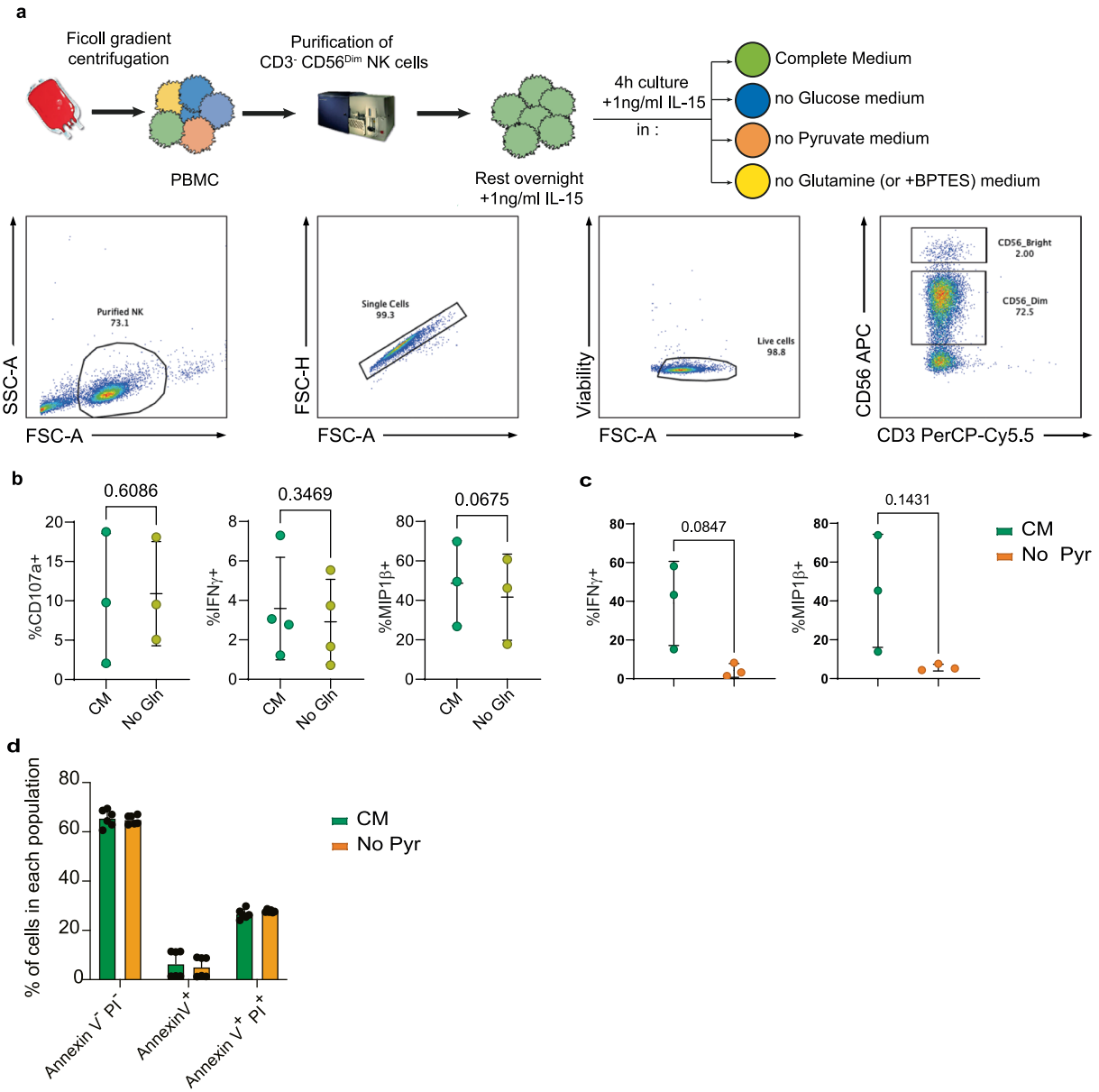

Extended Data Fig. 1 | (**a**) Model depicting the experimental set-up. (**b**) Sorted CD56^{Dim} NK cells were pre-incubated in the presence or absence of extracellular glutamine for 3 hours and stimulated for 4 hours with K562 cells expressing the nanoluc. The proportion of cells expressing CD107a, IFN-γ and MIP1-β was measured by flow cytometry. The proportion of positive cells (Mean +/-SD, n = 3 independent donors) is shown. (**c**) Sorted CD56^{Dim} NK cells were pre-incubated in the presence or absence of extracellular pyruvate for 3 hours and stimulated with IL-12/IL-18 cells for 4 hours. The proportion of cells expressing IFN-γ and MIP1-β was measured by flow cytometry. The proportion of positive cells (Mean +/-SD, n = 3 independent donors) is shown. (**d**) Sorted CD56Dim NK cells were cultured for 4 hours in the presence or absence of pyruvate with 1 ng/ml IL-15. Annexin V was labelled according to manufacturer's instructions (BD kit). PI was added extemporaneously, and cells were analysed by flow cytometry. The percentage of cells (Mean +/-SD; 2 independent donors) in the indicated cell populations is shown. Two-tailed T-test were performed comparing the indicated conditions in panel **b**, and **c**. Exact p-values are shown.

https://doi.org/10.1038/s42255-024-01188-4

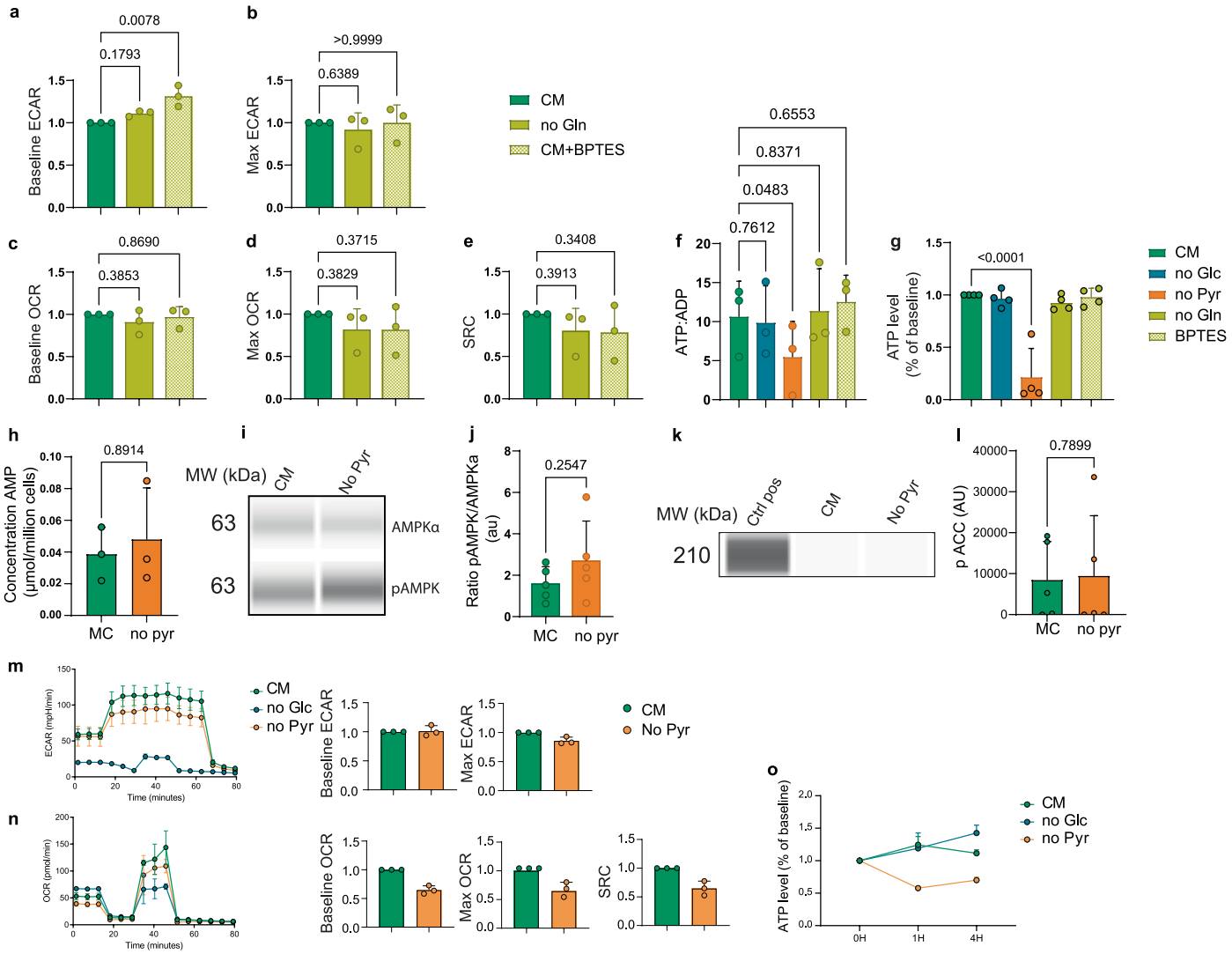

Extended Data Fig. 2 | (**a**) Sorted CD56^{Dim} NK cells were cultured in the indicated medium for 4 h. ECAR (**a-b**) and OCR (**c-e**) were measured. The results (Mean +SD) obtained from 3 independent donors are shown. ATP/ADP ratio (**f**) or ATP levels (**g**) in sorted CD56^{Dim} NK cells cultured in the indicated medium for 4 h was measured and is shown (Mean +SD, n = 3 or 4 independent donors). (**h-l**) Sorted CD56^{Dim} NK cells were cultured in the presence or absence of pyruvate for 4 h. (**h**) Absolute AMP concentration measured by mass spectrometry is shown (Mean +SD, n = 3 independent donors). The expression of AMPKα and p-AMPK (**i-j**) or p-ACC S79 (**k-l**) was measured by capillary WB. A representative image (**i** and **k**) or the result of the quantification (**j** and **l**) are shown (Mean +SD, n = 5 independent donors). For p-ACC quantification, sorted NK cells were treated for 1 h with MK8722, an activator of AMPK, to obtain a positive control (**l**). (**m-n**) In vitro activated NK cells were cultured in the indicated medium for 4 h. ECAR (**m**) and OCR (**n**) were measured. Left panels: One representative experiment (Mean +SD) out of three is shown. Right panels: individual points representing independent experiments are shown. (**o**) Sorted CD56^{Dim} NK cells were cultured in the indicated medium and the ATP level (Mean +SD, n = 6 independent donors) measured at the indicated time points are shown. One-way ANOVAs were performed with corrections for multiple testing in panels **a**, **b**, **c**, **d**, **e**, and **f**. Two-tailed T-test were performed comparing the indicated conditions in panel **g**, **h**, **j**, and **l**. Exact p-values are shown.

https://doi.org/10.1038/s42255-024-01188-4

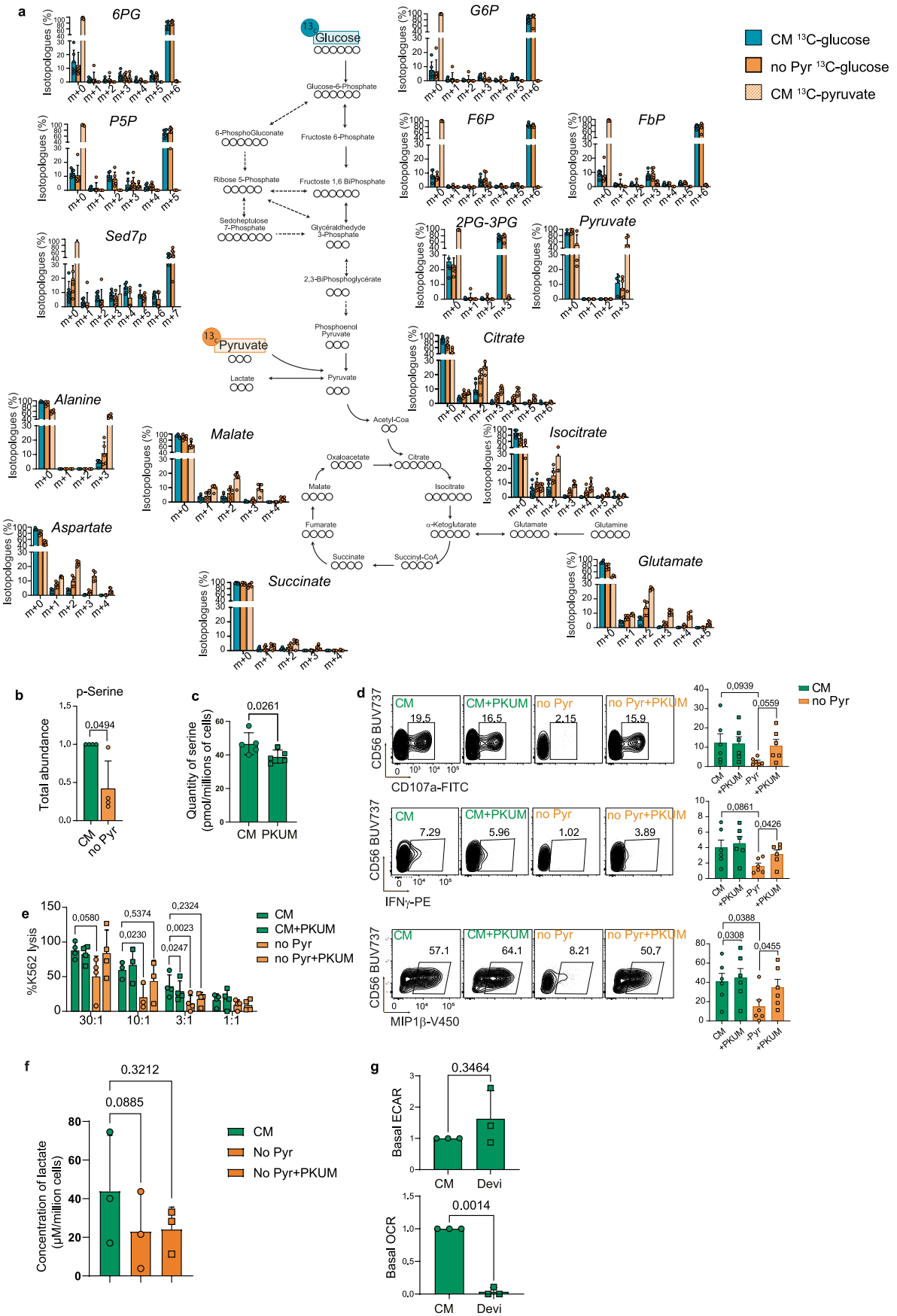

Extended Data Fig. 3 | See next page for caption.

https://doi.org/10.1038/s42255-024-01188-4

Extended Data Fig. 3 | (**a**) Sorted $CD56^{Dim}$ NK cells were cultured for 4 hours in the indicated medium. Mass isotopologue distribution after culture with ^{13}C-glucose (complete medium: in blue, without pyruvate: in orange) or ^{13}C-pyruvate (complete medium: light orange framed) for the indicated metabolites (n = 6 independent donors, values obtained for each individual donor are shown) measured by mass-spectrometry is shown. (**b**) The concentration of intracellular p-serine in sorted $CD56^{Dim}$ NK cells determined by MS after a 4-hour culture in the indicated medium is shown (n = 3 independent donors, values obtained for each individual donor are shown). (**c**) Intracellular serine concentration in *in vitro* activated NK cells cultured for 4 h in the presence or absence of PKUM was measured using a kit (Sigma) and is shown (Mean +SD, n = 5 independent donors). (**d**) Sorted $CD56^{Dim}$ NK cells were pre-incubated in medium +/− pyruvate +/− PKUM for 3 hours and incubated for 4 hours with K562 cells expressing the nanoluc. The proportion of cells expressing CD107a, IFN-γ and MIP1-β was measured by flow cytometry. Representative dot-plots (left panel) and the proportion of positive cells (Mean + SEM) for each experiment (right panel, n = 6 independent donors) are shown. (**e**) The percentage of K562 lysis (mean + SEM, n = 4 independent donors) is shown for the indicated E:T ratio. (**f**) Total abundance of lactate in supernatant of NK cells cultured for 3 h with or without pyruvate and PKUM were measured by RMN. Absolute quantities (Mean +SD, n = 3 independent donors) are shown. (**g**) Sorted $CD56^{Dim}$ NK cells were cultured in the presence or absence of Devimistat for 4 h. Basal ECAR and OCR were measured. The results (Mean +SD) obtained from 3 independent donors are shown. Individual points representing independent donors are shown in all panels. One-way ANOVAs were performed with corrections for multiple testing in panels **d**, **e**, and **f**. Two-tailed T-test were performed comparing the indicated conditions in panel **b**, **c**, and **g**. Exact p-values are shown.

https://doi.org/10.1038/s42255-024-01188-4

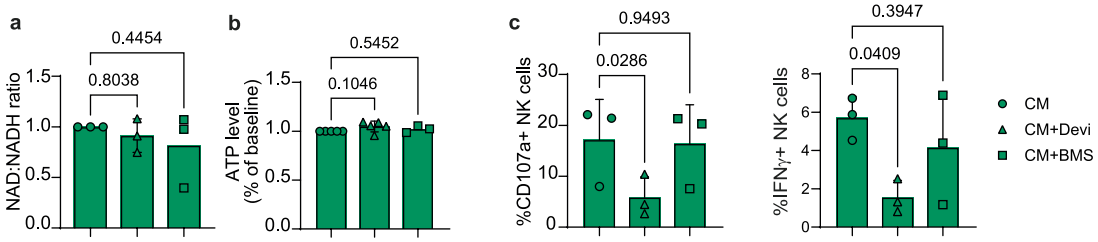

Extended Data Fig. 4 | Sorted CD56^{Dim} NK cells were cultured for 4 hours in complete medium in the presence or absence of Devimistat or BMS 303141. (**a**) NAD/NADH ratio, (**b**) ATP level or (**c**) the proportion of cells expressing CD107a, IFN-γ and MIP1-β measured by flow cytometry after K562 stimulation are shown (Mean +SD, n = 3 independent donors). One-way ANOVAs were performed with corrections for multiple testing in all panels. Exact p-values are shown.

https://doi.org/10.1038/s42255-024-01188-4

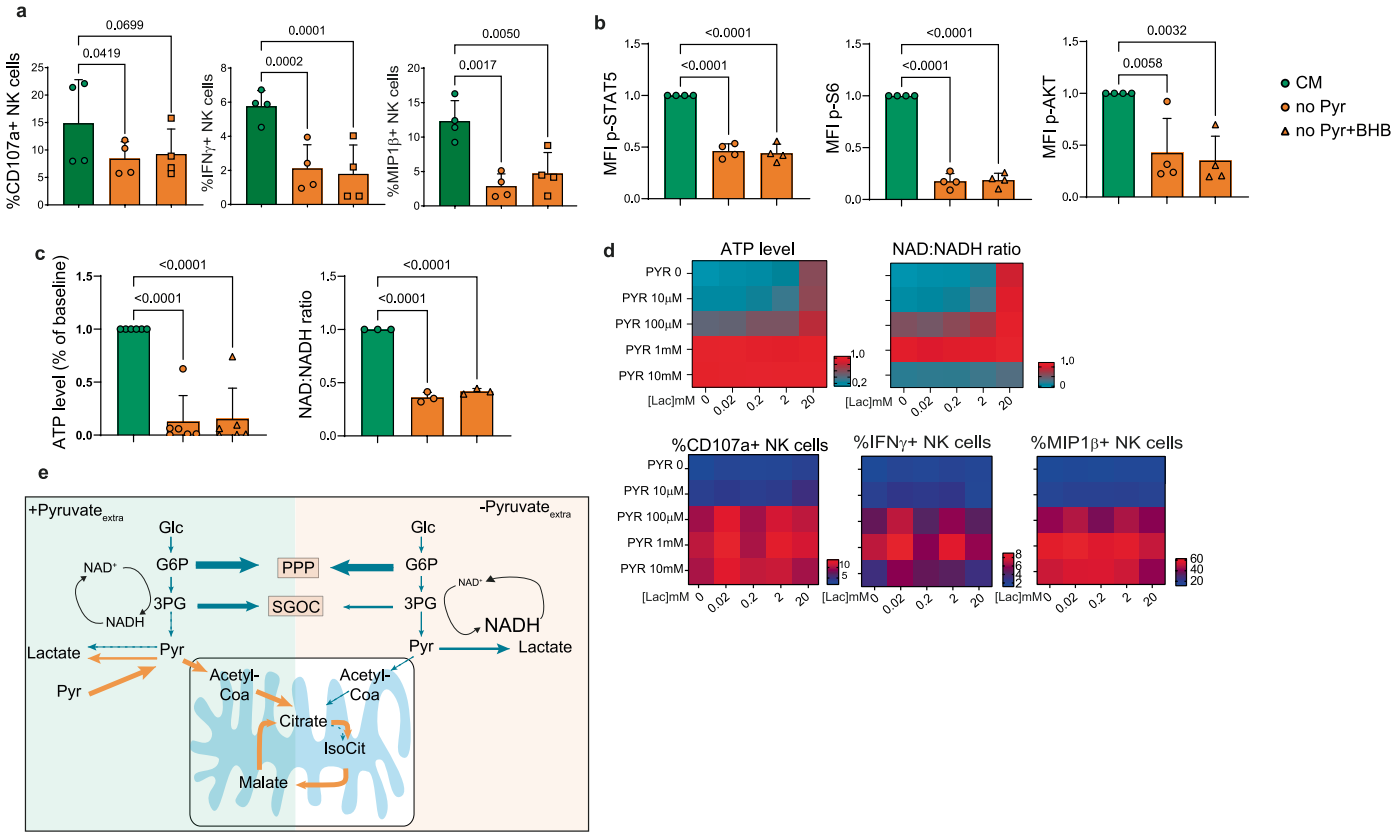

Extended Data Fig. 5 | (**a**) Sorted CD56^{Dim} NK cells were cultured for 3 hours in medium containing or not pyruvate and β-Hydroxybutyrate (BHB). The proportion of cells expressing CD107a, IFN-γ and MIP1-β measured by flow cytometry after stimulation with K562 is shown (Mean +SD, n = 4 independent donors). Sorted CD56^{Dim} NK cells were cultured for 4 hours in the indicated medium. (**b**) The Mean Fluorescence Intensity (MFI) for p-STAT5, p-S6 and p-AKT S473 was measured by flow cytometry and normalized to the complete medium (CM) condition for each experiment. The normalized MFI (Mean +SD) in independent donors (n = 4) is shown. (**c**) ATP level and NAD/NADH ratio were measured and normalized to the complete medium condition and are shown (Mean +SD, n = 3 independent donors for NAD/NADH ratio and 6 independent donors for ATP levels). (**d**) Sorted CD56^{Dim} NK cells were cultured for 4 hours in the indicated medium. ATP level and NAD/NADH ratio are shown (upper panel). The proportion of cells expressing CD107a, IFN-γ and MIP1-β measured by flow cytometry after K562 stimulation is shown (lower panel). Heatmaps depicting the results are shown (n = 3 independent donors for ATP and NAD/NADH ratio and n = 1 for functional parameters). (**e**) Model summarizing the principal findings of this study. See text for details. Blue and orange arrows represent metabolic pathways fed by glucose or pyruvate respectively. One-way ANOVAs were performed with corrections for multiple testing in panels **a**, **b**, and **c**. Exact p-values are shown.

QUERY FORM

Manuscript ID	**[Art. Id: 1188]**
Author	**Nicolas Kern**

AUTHOR:

The following queries have arisen during the editing of your manuscript. Please answer by making the requisite corrections directly in the e.proofing tool rather than marking them up on the PDF. This will ensure that your corrections are incorporated accurately and that your paper is published as quickly as possible.

Query No.	*Nature of Query*
Q1:	Your paper has been copy edited. Please review every sentence to ensure that it conveys your intended meaning; if changes are required, please provide further clarification rather than reverting to the original text. Please note that formatting (including hyphenation, Latin words, and any reference citations that might be mistaken for exponents) has been made consistent with our house style.
Q2:	Please check your article carefully, coordinate with any co-authors and enter all final edits clearly in the eproof, remembering to save frequently. Once corrections are submitted, we cannot routinely make further changes to the article.
Q3:	Note that the eproof should be amended in only one browser window at any one time; otherwise changes will be overwritten.
Q4:	Author surnames have been highlighted. Please check these carefully and adjust if the first name or surname is marked up incorrectly, as this will affect indexing of your article in public repositories such as PubMed. Also, carefully check the spelling and numbering of all author names and affiliations, and the corresponding author(s) email address(es). Please note that email addresses should only be included for designated corresponding authors, and you cannot change corresponding authors at this stage except to correct errors made during typesetting.
Q5:	You cannot alter accepted Supplementary Information files except for critical changes to scientific content. If you do resupply any files, please also provide a brief (but complete) list of changes. If these are not considered scientific changes, any altered Supplementary files will not be used, only the originally accepted version will be published.
Q6:	Please check Figures for accuracy as they have been relabelled. Please markup minor changes in the eProof. For major changes, please provide revised figures. (Please note that in the eProof the figure resolution will appear at lower resolution than in the pdf and html versions of your paper.)
Q7:	If applicable, please ensure that any accession codes and datasets whose DOIs or other identifiers are mentioned in the paper are scheduled for public release as soon as possible, we recommend within a few days of submitting your proof, and update the database record with publication details from this article once available.

QUERY FORM

Manuscript ID	**[Art. Id: 1188]**
Author	**Nicolas Kern**

AUTHOR:

The following queries have arisen during the editing of your manuscript. Please answer by making the requisite corrections directly in the e.proofing tool rather than marking them up on the PDF. This will ensure that your corrections are incorporated accurately and that your paper is published as quickly as possible.

Query No.	*Nature of Query*
Q8:	Please note, we reserve 'significant' and its derivatives for statistical significance. Please reword where this is not the intended meaning (for example to important, notable, substantial); there are 8 instances throughout your text.
Q9:	The parent figure of the source data file was changed from Fig. 1 to Fig. 3 based on the file description. Please confirm.
Q10:	Please confirm that the edits to the sentence 'Of note, the ECAR is indeed an indicator of glycolytic activity….' preserve the originally intended meaning.
Q11:	The text '(hereafter PKUM)' was added after the first instance of 'PKUMDL-WQ-2101' in the text. Correct definition?
Q12:	In the sentence beginning 'Interestingly, labelling was limited to citrate,…', please confirm that the insertion of '(CMS)' as the abbreviation for 'citrate–malate shuttle' is correct'.
Q13:	In the sentence beginning 'Pyruvate can enter the TCA by carboxylation…', please confirm that the insertion of 'pyruvate dehydrogenase' as the definition of 'PDH' is correct'.
Q14:	In Fig. 3 caption, the two instances of RMN was changed to NMR. Correct change? If not, please replace the abbreviation with the full name.
Q15:	Please confirm the definitions of abbreviations at the end of FIg. 3 caption.
Q16:	Please confirm that the edits to the sentence '…BMS-303141 similarly had no effect on the NAD/NADH ratio.' preserve the originally intended meaning.
Q17:	In Fig. 5e caption, please confirm that the edits to the sentence 'The proportion of cells positive for CD107a, IFNγ and MIP1β measured by flow cytometry….' preserve the originally intended meaning. Here, 'MIP1β' was added to the description to match the graphic.
Q18:	In Fig. 5 caption, please confirm that the grouping of descriptions for panels a,b, c,d, and f–h is correct.

QUERY FORM

Manuscript ID	**[Art. Id: 1188]**
Author	**Nicolas Kern**

AUTHOR:

The following queries have arisen during the editing of your manuscript. Please answer by making the requisite corrections directly in the e.proofing tool rather than marking them up on the PDF. This will ensure that your corrections are incorporated accurately and that your paper is published as quickly as possible.

Query No.	*Nature of Query*
Q19:	The sentence 'In this study, we addressed the fuel requirements of resting NK cells.' has been edited to remove the priority claim, according to style. Please check and confirm.
Q20:	Please confirm that the edits to the sentence '…, with PIK3δ—the PI3K isoform expressed in lymphocytes—presenting an elevated K_m for ATP' preserve the originally intended meaning.
Q21:	'Murine' means 'mice and related rodents' (including rats). There are 3 instances of 'murine' in the paper when citing previous studies. Please change to 'mouse' when referring specifically to mice.
Q22:	Reference 29 was not originally cited in the text. Please confirm that the citation of this reference after the sentence 'Other regulatory steps, such as post-translational activation of…' is ok.
Q23:	Please confirm that the edits to the sentence 'Citrate levels are restored by SGOC inhibition, supporting the hypothesis that….' preserve the originally intended meaning.
Q24:	Please confirm that the edits to the sentence 'In addition, inhibition of PHGDH rescued ATP levels….' preserve the originally intended meaning.
Q25:	Please confirm that the edits to the sentence '…whereas overt stimulation would lead to activation.' preserve the originally intended meaning.
Q26:	Please confirm that the edits to the sentence 'Furimazine was generated from a hikarazine….' preserve the originally intended meaning.
Q27:	Please confirm that the edits to the sentence 'The samples were then recovered with 100 µl MilliQ water….' preserve the originally intended meaning.
Q28:	Please confirm that the edits to the sentence 'The gradient programme started with 2% solvent B….' preserve the originally intended meaning.
Q29:	Figure legends should begin with a brief title for the whole figure as the first sentence, then continue with a caption containing a short description of each panel and the symbols used. Please provide the missing title for Extended Data Figs. 1–5.

QUERY FORM

Manuscript ID	**[Art. Id: 1188]**
Author	**Nicolas Kern**

AUTHOR:

The following queries have arisen during the editing of your manuscript. Please answer by making the requisite corrections directly in the e.proofing tool rather than marking them up on the PDF. This will ensure that your corrections are incorporated accurately and that your paper is published as quickly as possible.

Query No.	*Nature of Query*
Q30:	In the Acknowledgements, please confirm that the edits to the sentence 'N.K. was an employee of Parfums Christian Dior (thèse CIFRE) at the time of the study.' preserve the originally intended meaning.
Q31:	Please check that all funders have been appropriately acknowledged and that all grant numbers are correct.
Q32:	Please check that the Competing Interests declaration is correct as stated. If you declare competing interests, please check the full text of the declaration for accuracy and completeness.
Q33:	For ref. 22, the article title was changed to the final published form. Please confirm.

nature portfolio

Corresponding author(s): Antoine Marçais

Last updated by author(s): Oct 30, 2024

Reporting Summary

Nature Portfolio wishes to improve the reproducibility of the work that we publish. This form provides structure for consistency and transparency in reporting. For further information on Nature Portfolio policies, see our Editorial Policies and the Editorial Policy Checklist.

Statistics

For all statistical analyses, confirm that the following items are present in the figure legend, table legend, main text, or Methods section.

n/a	Confirmed	
☐	☒	The exact sample size (*n*) for each experimental group/condition, given as a discrete number and unit of measurement
☐	☒	A statement on whether measurements were taken from distinct samples or whether the same sample was measured repeatedly
☐	☒	The statistical test(s) used AND whether they are one- or two-sided *Only common tests should be described solely by name; describe more complex techniques in the Methods section.*
☒	☐	A description of all covariates tested
☒	☐	A description of any assumptions or corrections, such as tests of normality and adjustment for multiple comparisons
☐	☒	A full description of the statistical parameters including central tendency (e.g. means) or other basic estimates (e.g. regression coefficient) AND variation (e.g. standard deviation) or associated estimates of uncertainty (e.g. confidence intervals)
☐	☒	For null hypothesis testing, the test statistic (e.g. *F*, *t*, *r*) with confidence intervals, effect sizes, degrees of freedom and *P* value noted *Give P values as exact values whenever suitable.*
☒	☐	For Bayesian analysis, information on the choice of priors and Markov chain Monte Carlo settings
☒	☐	For hierarchical and complex designs, identification of the appropriate level for tests and full reporting of outcomes
☒	☐	Estimates of effect sizes (e.g. Cohen's *d*, Pearson's *r*), indicating how they were calculated

Our web collection on statistics for biologists contains articles on many of the points above.

Software and code

Policy information about availability of computer code

Data collection	Microsoft Excel 16.90
Data analysis	Prism 9.5.1

For manuscripts utilizing custom algorithms or software that are central to the research but not yet described in published literature, software must be made available to editors and reviewers. We strongly encourage code deposition in a community repository (e.g. GitHub). See the Nature Portfolio guidelines for submitting code & software for further information.

Data

Policy information about availability of data

All manuscripts must include a data availability statement. This statement should provide the following information, where applicable:

- Accession codes, unique identifiers, or web links for publicly available datasets
- A description of any restrictions on data availability
- For clinical datasets or third party data, please ensure that the statement adheres to our policy

Data that support the findings of this study are available upon request from the corresponding authors AM or TW. A Source Data file containing the uncropped blots shown if Fig. 3g is available online.

Research involving human participants, their data, or biological material

Policy information about studies with human participants or human data. See also policy information about sex, gender (identity/presentation), and sexual orientation and race, ethnicity and racism.

Reporting on sex and gender	This information has not been collected. Sex and gender were not considered in the study design.
Reporting on race, ethnicity, or other socially relevant groupings	This information has not been collected.
Population characteristics	Samples only came from healthy donors. Other population characteristics were not collected.
Recruitment	Participants were voluntary donors, not recuited specifically for this study. Peripheral blood samples from healthy subjects were obtained from the French blood agency (Etablissement Français du sang, Lyon, France) after donor's informed consent had been obtained.
Ethics oversight	The research reported in this study complies with all relevant French ethical regulations.

Note that full information on the approval of the study protocol must also be provided in the manuscript.

Field-specific reporting

Please select the one below that is the best fit for your research. If you are not sure, read the appropriate sections before making your selection.

☒ Life sciences ☐ Behavioural & social sciences ☐ Ecological, evolutionary & environmental sciences

For a reference copy of the document with all sections, see nature.com/documents/nr-reporting-summary-flat.pdf

Life sciences study design

All studies must disclose on these points even when the disclosure is negative.

Sample size	We did not perform sample size calculations as we did not know what to expect in terms of difference. We tried to analyze at least 3 independent samplesin eachgroup for all measurements.We hadto balancethe difficulty to obtain sufficient amount of resting NKcells l (limited number of voluntary donors, ethical issue of using blood products ...) with the necessity to repeat the experiments, 3 independent replicates (independent donors and day of experiment) seemed an appropriate compromise.
Data exclusions	No data were excluded.
Replication	For all experiments, at least 3 biological replicates (donors) and up to 17 were used. Replicates are all shown.
Randomization	Only blood samples from healthy donors were used, no randomization could be performed at this stage (ie all experimental conditions were tested for a given donor).
Blinding	The metabolomic measurement were performed in a totally blinded fashion. For other experiments, such asSeahorseor flow-cytometry, no blinding was involved, as machine-based readouts are not subject to investigator bias.

Reporting for specific materials, systems and methods

We require information from authors about some types of materials, experimental systems and methods used in many studies. Here, indicate whether each material, system or method listed is relevant to your study. If you are not sure if a list item applies to your research, read the appropriate section before selecting a response.

Materials & experimental systems

n/a	Involved in the study
☐	☒ Antibodies
☐	☒ Eukaryotic cell lines
☒	☐ Palaeontology and archaeology
☒	☐ Animals and other organisms
☒	☐ Clinical data
☒	☐ Dual use research of concern
☒	☐ Plants

Methods

n/a	Involved in the study
☒	☐ ChIP-seq
☐	☒ Flow cytometry
☒	☐ MRI-based neuroimaging

Antibodies

Antibodies used

The following mAbs were used for flow cytometry:
anti-CD56 APC (BD Biosciences; clone NCAM16.2) 1/50 https://www.bdbiosciences.com/en-fr/products/reagents/flow-cytometry-reagents/clinical-diagnostics/single-color-antibodies-asr-ivd-ce-ivd/cd56-apc.341027

anti-CD3 PerCP-Cy5.5 (BD Biosciences; clone UCHTl) 1/50 https://www.bdbiosciences.com/en-fr/products/reagents/flow-cytometry-reagents/research-reagents/single-color-antibodies-ruo/rb705-mouse-anti-human-cd3.570237

anti-pSTAT5 A488 (BD Biosciences clone 47/StatS(pY694)) 1/40 https://www.bdbiosciences.com/en-fr/products/reagents/flow-cytometry-reagents/research-reagents/single-color-antibodies-ruo/alexa-fluor-488-anti-stat5-py694.562075

anti-pS6 PE (Cell Signaling Technologies clone D57.2.2E) 1/400https://www.cellsignal.com/products/antibody-conjugates/phospho-s6-ribosomal-protein-ser235-236-d57-2-2e-xp-rabbit-mab-pe-conjugate/5316

anti-pAKT PECF594 {BD Biosciences clone M89-61) 1/100 https://www.bdbiosciences.com/en-fr/products/reagents/flow-cytometry-reagents/research-reagents/single-color-antibodies-ruo/pe-cf594-mouse-anti-akt-ps473.562465

anti-lFN-g PE (Biolegend, clone 4S.B3) 1/10 https://www.biolegend.com/fr-fr/products/pe-anti-human-ifn-gamma-antibody-1011

anti-CD107a FITC (BD Biosciences clone H4A3) 1/50 https://www.bdbiosciences.com/en-fr/products/reagents/flow-cytometry-reagents/research-reagents/single-color-antibodies-ruo/fitc-mouse-anti-human-cd107a.555800

anti-MIP1b BV421 (BD Biosciences clone D21-1351) 1/20 https://www.bdbiosciences.com/en-fr/products/reagents/flow-cytometry-reagents/research-reagents/single-color-antibodies-ruo/bv421-mouse-anti-human-mip-1.562900

For capillary western-blot, the following Ab were used:
Anti-PHGDH rabbit (NBP1-87311; Novus Biologicals Europe) 1/80 https://www.novusbio.com/products/phgdh-antibody_nbp1-87311

anti-LDHA rabbit (NBP1-48336; Novus Biologicals Europe) 1/200 https://www.novusbio.com/products/lactate-dehydrogenase-a-ldha-antibody_nbp1-48336

anti-LDHB rabbit (MAB9205-SP, R&D Systems) 1/250 https://www.novusbio.com/products/lactate-dehydrogenase-b-antibody-2057d_mab9205

anti-AMPKa (D5A2, CST) 1/50 https://www.cellsignal.com/products/primary-antibodies/ampka-d5a2-rabbit-mab/5831

anti-pAMPK Thr172 (40H9, CST) 1/10 https://www.cellsignal.com/products/primary-antibodies/phospho-ampka-thr172-40h9-rabbit-mab/2535

anti-pACC Ser79 (3661, CST) 1/50 https://www.cellsignal.com/products/primary-antibodies/phospho-acetyl-coa-carboxylase-ser79-antibody/3661

Validation

Ali antibodies used in this study are commercially available, and all have been validated by the manufacturers and used by other publications. This information is provided on their website (see links above) and product information datasheets. We titrated these antibodies l according to our own staining conditions.

Eukaryotic cell lines

Policy information about cell lines and Sex and Gender in Research

Cell line source(s)

K562-Nanoluc cells (stored in out institute).

Authentication

We derived this cell line from the commercially available K562 cell line (ATCC:CCL243). After derivation, this cell line was not further authentificated.

Mycoplasma contamination

Ali cell lines tested negative for mycoplasma, and we used a commercial kit to make sure of it (Lonza MycoAlert kit)# J LT07-418.

Commonly misidentified lines
(See ICLAC register)

No commonly misidentified cell lines were used in the study.

Plants

Seed stocks	N/A
Novel plant genotypes	N/A
Authentication	N/A

Flow Cytometry

Plots

Confirm that:

☒ The axis labels state the marker and fluorochrome used (e.g. CD4-FITC).

☒ The axis scales are clearly visible. Include numbers along axes only for bottom left plot of group (a 'group' is an analysis of identical markers).

☒ All plots are contour plots with outliers or pseudocolor plots.

☒ A numerical value for number of cells or percentage (with statistics) is provided.

Methodology

Sample preparation	Human PBMCswere separated from peripheral blood by Ficoll gradient centrifugation (Eurobio Laboratoires et AbCys)at room temperature (RT).PBMCwere kept at 4°Cin complete medium overnight. Forisolation of CD56DimNKcells,afirst stepof enrichment wasperformed usinganNKcellisolation Kit(Miltenyi Biotec) following manufacturer's instructions. CD56Dim CD3- NK cells were then sorted (BD FACSARIA II, purity > 99%).
Instrument	Flow cytometry analysiswas performed on a Becton-Dickinson FACSLSRIIFortessa;cell sorting was performed on an Becton-DickinsonAria II.
Software	Datawere analyzedwith FlowJo10.9.0software (TreeStar).
Cell population abundance	For CD56Dim NK cell sorting, 98-100% purity was obtained, as measured by flow cytometry upon re-acquisition of the purified samples. I For NKcell purification, >97% purity was obtained, as measured by flow cytometry upon re-acquisition of the purified samples.
Gating strategy	For all experiments, sorted cells were gated as CD56Dim/CD3-.

☒ Tick this box to confirm that a figure exemplifying the gating strategy is provided in the Supplementary Information.